E-20-K79
#1

Flow Test Evaluation

- Final Research Report-

Submitted to :
Georgia Department of Transportation

J. Carlos Santamarina (PI)
Douglas Cortes
Hyun-Ki Kim
Angelica M. Palomino

Civil and Environmental Engineering
Georgia Institute of Technology

February 2006

TABLE OF CONTENTS

Part I. Introduction

The use of manufactured sands in Portland Cement Concrete (PCC) has increased, especially in areas where natural sands are scarce. Production of crushed stone, sand and gravel in the United States has grown from about 0.2 billion tones in 1940 to 1.84 billion tones in 1970 and 2.75 billion tons in 2001 (NSSGA).

Despite of the wider use of manufactured sands, current assessment methods are based on natural sand characteristics and performance for the most parts. It is postulated that enhanced evaluation procedures are required for the proper screening of manufactured sands. The conceptual framework for this study is to seek the most efficient utilization of materials while conforming to performance requirements for Portland cement concrete.

Specifications for concrete sand invariably consider grain size distribution. Other requirements may include, but are not limited to, acceptable test results for sand equivalency, durability, organic impurities, fineness modulus, and reactivity. Even though the sand from a particular source meets all these requirements, there is no guarantee that the sand will perform satisfactorily in concrete at the specified gradation. Other sand characteristics such as mineralogy, particle shape, and surface texture are not necessarily measured by typical tests. Yet, they may strongly influence overall performance (Quiroga and Fowler 2003). It is often not possible to meet all design and water demand requirements with a manufactured sand of a specified gradation. The Georgia Department of Transportation has two manufactured sand gradations. Yet, some manufactured sand sources satisfy either of the two gradations, but they fail to meet concrete design requirements. Conversely, the sand could perform satisfactorily even if graded outside the specified ranges. Therefore, reliance on a performance-based test procedure rather than on a

gradation specification may lead to the enhanced use of available materials and aggregate sources.

While current tests performed on concrete sands are designed to measure individual physical characteristics, procedures could be developed to directly assess sand suitability for use in concrete by taking into consideration the total influence of all physical characteristics. The ideal performance-based test for concrete sand would take into account the combined effect of the inherent characteristics of the sand such as surface area, particle shape, and surface texture, and grain size distribution that affect water demand, workability, and performance.

The main goal of this research is to assess the suitability of the flow test (ASTM C1437-01) as a performance-based discriminator of sands for PCC. The scope of the study includes a detailed characterization of selected aggregates, the fresh mortar, and the hardened mixture. In addition, we conduct an in-depth mechanical analysis of the flow test itself to gain insight into the underlying physical processes involved in this measurement, and its ability to capture fresh mortar rheology.

Part II. Literature Review

Despite the large number of publications that describe the rheological behavior of cement mortar, an unambiguous method to predict its rheology from the interaction between components (i.e. cement, water, fine aggregates, and entrapped air) has not been proposed yet. This highlights the complexity of this material. Several models have been proposed to capture the rheological properties of concrete and mortar flow: Newtonian, Bingham, Herschel and Bulkley, power equation, Vom Berg, Eyring, Robertson-Stiff, and Atzeni. The main objective of these models is to describe the shear stress and shearing rate of viscous flow. The Bingham model is the most commonly used (Ferraris, 1999; Tattersall and Banfill, 1983; Banfill, 1994; See Figure 2.1). The two parameters in this model, yield stress and plastic viscosity, can be independently obtained. Plastic viscosity is the parameter that controls pumpability and ease of finishing (Ferraris and de Larrard 1998).

Although the modeling tools are relatively well established, current field tests fail to measure the appropriate parameters. While some tests can measure the yield stress, they all fail to assess plastic viscosity. Modifications to the slump test have been proposed to include measurements of time for partial slumps to address this issue (Ferraris and de Larrard 1998).

2.1 Role of Cement Paste in Mortar

Cement paste acts as a separator for larger aggregates in mortar (Ferraris and Gaidis 1992). The lack of sufficient mortar results in a mixture of limited flow, prone to segregation, and difficult to finish (Bodenlos and Fowler 2003).

2.2 Grain Size Distribution

Non-plastic fines in a concrete mix affect its workability, shrinkage, density, stiffness, and strength (Regourd 1976; Jackson 1996; Schiller 1992; Schimdt 1992):

- Fines control the gaps in the finer portion of the particle size distribution.
- The finer particles displace some of the water from voids within the coarser material. Thus, lesser water is necessary to coat aggregates.
- Lesser use of water increases the strength of the hardened concrete due to reduction of effective water content.

The favorable effect of the non-plastic limestone fines in the grain size distribution enhances the rheology of cement mortar; on the contrary, the presence of clay particles within the material increases water demand (Cochet and Sorentino 1993), and more fines may require additional admixtures to improve workability because fines have higher specific surface that must be coated by cement paste in order to attain enough workability (Quiroga and Fowler 2004).

Due to economical and environmental issues regarding the fines produced during mining and crushing, many countries have already done (or are in the process of) revising their regulations to permit higher fine contents in construction materials (Fowler and Constantino 1997). The American Cement Industry is in the process of obtaining a revision of the ASTM C150 standard to incorporate five percent crushed limestone (Zollinger and Sarkar 2001).

2.3 Particle Shape

The geometry of aggregates is evaluated in terms of roundness, sphericity and

surface roughness. The shape of sand particles may be traced back to the crystallization process of cooling magma. Subsequent cleavage and abrasion is responsible for roundness and roughness. Rounder, more spherical, and smoother particles promote lower maximum and minimum void ratios, and a smaller gap between the two extreme void ratios (Santamarina and Cho 2004). Particle shape influences other key aspects of granular systems behavior such as stiffness, strength, evolution of anisotropy, dilation, and the development of strain localization (Dodds 2003).

Rock crushing creates a material with distinctive particle shape, which depends on the parent rock composition, mode of fracture, coordination number during crushing, and the ratio of grain size to product size. The general outcome of the crushing process is an angular material. The angular nature of crushed sands leads to lower small strain stiffness, and higher critical state friction angles when compared with more rounded natural sands (Dodds 2003). Angular particles lead to mixtures with lower workability than cubical or spherical sands for a given water content (Quiroga and Fowler 2003). In order to improve workability water is often incorporated, yet higher water content results in lower strength, even though angular particles themselves increase strength (Kaplan 1959).

2.4 Mixing Method – Cement Clumps

An ideal cement paste should be free of cement clumps, and every single particle should be surrounded by water (Williams et al. 1999), yet even fresh bags of cement contain clumps. These agglomerates have been attributed to attractive forces such as electrostatic or van der Waals, or due to bonding between particles caused by natural

moisture in air (Yang and Jennings 1995). The presence of agglomerated particles has been known to be detrimental to flow. The particle clusters share a single hydration membrane that may be broken by increasing shear. Therefore, the rheological properties of mortar are highly sensitive to the mixing method; more efficient breakage of cement clumps leads to better flow (Williams et al. 1999). It has been further suggested that cement particles within the clusters remain unhydrated for at least five hours or even longer, and are likely responsible for microstructural defects unfavorable to the strength of the hardened mixture (Yang and Jennings 1995).

2.5 Flow Evaluation Tests

The previously standardized flow test (ASTM C124-71) was withdrawn once in 1973 because its use in the field was deemed cumbersome compared to the slump test described in ASTM C143 (Roy and Idorn 1993). It was later revived as ASTM C1437-01 for its unique advantages, such as reproductivity and standardization. Still, flow test results remain difficult to interpret. Therefore the test is currently used as a qualitative index of workability.

Various tests employ vibration to measure the rheological properties of cement mixtures: compaction test (Walz test), Vebe consistometer, Powers remolding test, Thaulow tester, flow table test (DIN flow table), Angels flow box test, LCL flow test, Wigmore consistometer, vibropenetrator, inverted slump cone test, vertical pipe apparatus, vibrating slope apparatus, settlement column segregation test, and vibratory flow meter (Koehler and Fowler 2003). The flow table test (DIN flow table; DIN 1048; BS EN 12350-5) is the

closest to the flow test (ASTM C1437-01): A cone-shaped mold is used, multiple jolts (drops) at a given height are applied to spread the mortar, and the horizontal spread of the mortar is measured. Previous researchers have concluded that (Diamond and Bloomer 1977; Mor and Ravina 1986; Tattersall 1991; Bartos 1992; Koehler and Fowler 2003):

- This test is simple, inexpensive, and can be readily available in the field.
- Test results are difficult to analyze, and are not adequate to investigate shear rate effects.
- The spread of fresh concrete becomes homogenized as the number of jolts increases.
- The initial spread and the final spread after 15 jolts correlate linearly, yet the initial spread is more sensitive than the final spread.
- A nonlinear relationship is obtained between the spread of cement mortar and the number of jolts.
- Concrete slump and final mortar spread correlate linearly when the concrete slump is greater than seven inches.

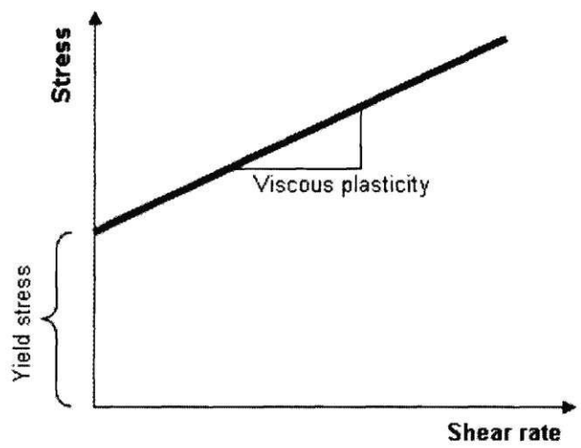

Figure 2.1 Bingham rheology model

Part III. An Experimental Study of the Flow Test

Mixtures are prepared with different mass fraction of round and rough angular particles to gain insight into the evolution of the flow test and the role of particle shape on the rheological properties of cement mortar.

3.1 Material Description

Two different sands are selected: Ottawa natural sand and crushed granite sand. Both sands have the same particle size range (0.85mm>D>0.60mm) to magnify the effect of surface texture (rather than grain size) on the rheological properties. The mixtures are prepared with different mass fractions of Ottawa natural sand: 0% (pure crushed granite sand), 10%, 20%, 30%, 40%, 50%, 70% and 100% (pure Ottawa natural sand). Gravimetric mixing ratios are kept constant: Fine aggregate to cement ratio (FA/C=2.0) and water to cement ratio (W/C=0.46). Mixing is implemented with a blending machine.

Ottawa sand is round, spherical and smooth, while crushed granite sand is angular, platier, and rough. Detailed surface roughness is observed using an optical microscope (Leica MZ6 stereomicroscope) or scanning electron microscope (SEM, Hitachi S-800 FEG SEM, See Figure 3.1). Figure 3.2a&c show more pronounced roughness and indentations on the surface of crushed granite sand than on Ottawa sand at a scale of about 100μm. Differences vanish at the 10μm scale (See Figure 3.2b&d). Therefore, crushing contributes to surface roughness in a scale of about 10% the particle diameter.

3.2 Test Procedure and Results

The flow test is performed following ASTM C1437-01. The procedures are described in Appendix A.7. The spread of the mortar on the table of the device is digitally photographed after each drop. Figure 3.3 shows the evolution of flow during the first 25 drops for the case of 100% Ottawa sand mortar. Flow test results for all mixtures are shown in Figure 3.4.

The DIN flow table test standard warns that the coarse aggregate can segregate from the mortar during vibrations, and it recommends recording the segregated area (Bartos 1992). Such segregation can occur between cement paste and fine aggregates and between round and rough particles. The deformed mortar pile (50% Ottawa natural sand and 50% crushed granite sand mixture) after 25 drops is divided into eight pieces as shown in Figure 3.5a. Sand composition is measured by washing away the paste. Results show that vibration in the flow test causes less than 1% segregation between paste and fine aggregates. Results are summarized in Table 3.1 and Figure 3.5b.

3.3 Analysis and Discussion

The flow test is a measure of horizontal spread that a cement mortar experiences due to successive dynamic impacts. The height of the mortar pile decreases with spread (wet mixtures preserve volume). As the height decreases, the driver for spreading decreases while the surface-mortar drag increases. Therefore, the incremental spread decreases with the number of drops. Consequently, the nonlinear flow F versus number of drops N trend (e.g. Figure 3.3b) is herein fitted with a hyperbolic equation.

$$F = \frac{N}{aN + b} \tag{3.1}$$

The two independent parameters a and b are replaced by the flow value at 25 drops A, and the initial flow rate B at the beginning of the test.

$$A = F\big|_{N=25} = \frac{25}{25a + b} \tag{3.2}$$

$$B = \frac{dF}{dN}\bigg|_{N=0} = \frac{b}{(aN + b)^2}\bigg|_{N=0} = \frac{1}{b} \tag{3.3}$$

The model parameters are fitted by minimizing the L_2 norm.

$$L_2 = \left[\sum_i \left| F_i^{<measured>} - F_i^{<estimated>} \right|^2 \right]^{1/2} \tag{3.4}$$

All the fitted data are shown in Figure 3.4. The A-parameter (flow at 25 drops) and the B-parameter (initial flow rate) are plotted versus mass fraction of the Ottawa natural sand in Figure 3.6. Both A and B increase with the percentage of natural aggregates. The correlation between A and B suggests that only one drop can be enough to characterize the flow as shown in Figure 3.7. However, detailed analysis of the measurements shows that spreads during the initial drops are considerably noisy.

Natural round particle begins exerting a strong effect on flow when mass fraction of natural particles ≥ 30-50%; therefore, the presence of natural round particles is more effective in promoting flow than the crushed particles in hindering it. Mixtures can be classified into round-like, crushed-like, and transitional mixtures. The transition range in this study is observed between 30% and 50% natural sand mixtures.

The hyperbolic fittings show that flow for all mixtures converges as the number of drops increases (See DIN flow table test). Therefore, the previous regression analysis can

be simplified by selecting a value of flow at an infinite number of drops. Then, the hyperbolic model is a function of only one parameter: the initial flow rate B-parameter. Results in this study suggest that the asymptotic flow be 200% (Figure 3.8). Then, Equation 3.1 becomes:

$$F = \frac{N}{0.5N + b^*} \tag{3.5}$$

where b^* is the inverse of an initial flow rate:

$$b^* = N_0 \left(\frac{1}{F|_{N=N_0}} - \frac{1}{2} \right) \tag{3.6}$$

The inverted values of b^* are plotted in Figure 3.9.

Flow is determined by frictional resistance at particle contacts. It is greatest between crushed particles and smallest between natural particles. Let's assume that the number of particles is infinite, and that there are no boundary effects. Then, if flow rate is inversely proportional to the summation of frictional resistances at each contact and the role of cement paste on mortar flow is ignored, a flow model based on contact friction can be proposed.

$$P(n_0, n_N, n_C, p_0) = P(n_N, p_0) = p_0^{n_N} \cdot (1 - p_0)^{n_C} \cdot \frac{n_0!}{n_N! n_C!} \tag{3.7}$$

$$\alpha_{eff} = \frac{1}{n_0} \sum_{n_N=0}^{n_0} P(n_N, p_0) \cdot [p_0 \cdot (\alpha_{NN} n_N + \alpha_{NC} n_C) + (1 - p_0) \cdot (\alpha_{NC} n_N + \alpha_{CC} n_C)] \tag{3.8}$$

$$B \propto 1/\alpha \tag{3.9}$$

where P is the probability that natural sand particles are attached on a certain particle, n_0 is

the nominal coordination number (assumed seven in this study), n_C is the number of crushed particles attached to the given particle, n_N is the number of natural sand particles attached to the given particle, p_0 is the volume fraction of natural particles, α is a flow resistance factor of a mortar defined as an inverse of a flow parameter, α_{NN} is one between natural particles, α_{NC} is one between natural and crushed particles, α_{CC} is one between crushed particles, and B is the one-parameter hyperbolic model parameter for flow.

Figure 3.9 shows the estimated hyperbolic model parameter B for all mixtures in the extreme cases that α_{NC} approaches α_{NN} (upper curve) or α_{CC} (lower curve). This model supports that a flow resistance between natural and crushed particles is much closer to the one between natural particles than the one between crushed particles, but the behavior of $p_0 \leq 0.2$ mixtures is overwhelmed by crushed particles. However, this model overestimates the contribution of crushed particle contacts to flow when $p_0 \geq 50\%$.

Table 3.1 Segregation in flow test after 25 blows: The target fine aggregate to paste ratio is 1.37 but the measured mean ratio is 1.49. Sand: 50% Ottawa 50% crushed granite.

Number of piece	Fine aggregate [g]	Cement paste [g]	FA/Paste
#1	60.91	41.02	1.48
#2	50.18	36.90	1.36
#3	62.01	40.25	1.54
#4	67.44	42.71	1.58
#5	27.21	18.23	1.49
#6	27.37	18.25	1.50
#7	37.09	22.28	1.66
#8	34.77	26.55	1.31

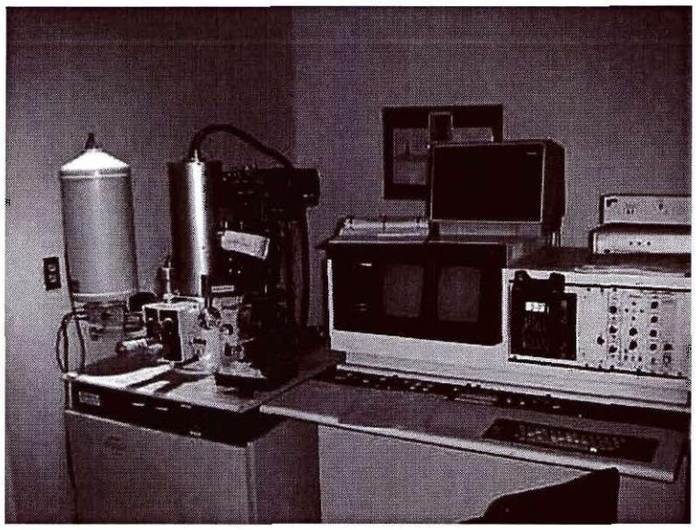

Figure 3.1 Hitachi S-800 Field Emission Gun Scanning Electron Microscope

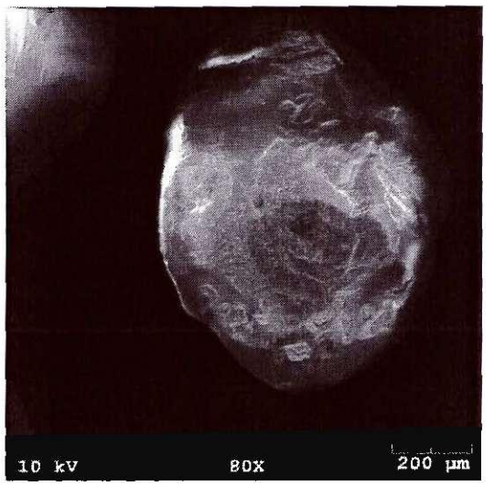

(a) Ottawa sand particle (X80)

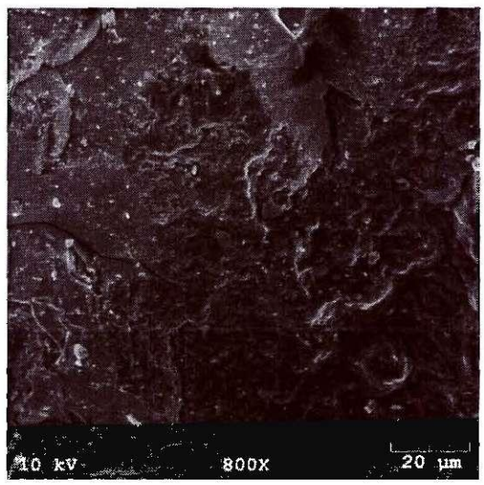

(b) Ottawa sand particle (X800)

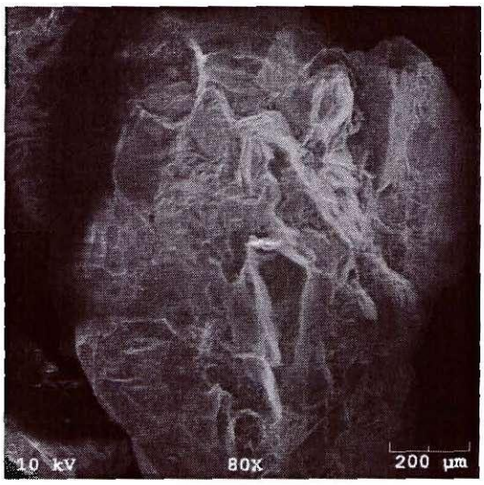

(c) Crushed granite particle (X80)

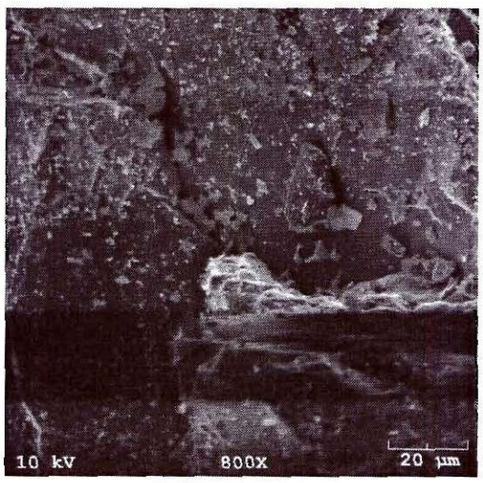

(b) Crushed granite particle (X800)

Figure 3.2 Scanning electron microscope pictures of Ottawa natural sand (a&b) and crushed granite sand (c&d).

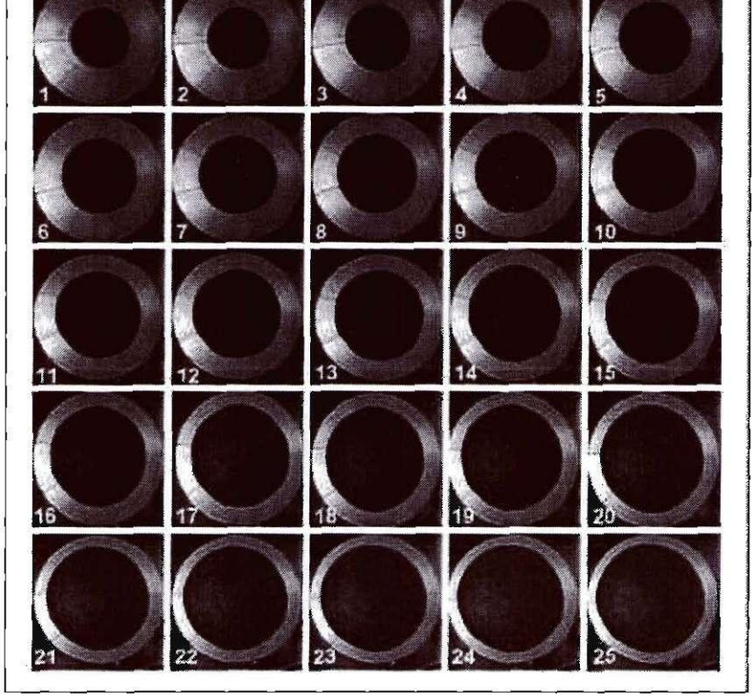

(a) Pictures of mortar spread with drops

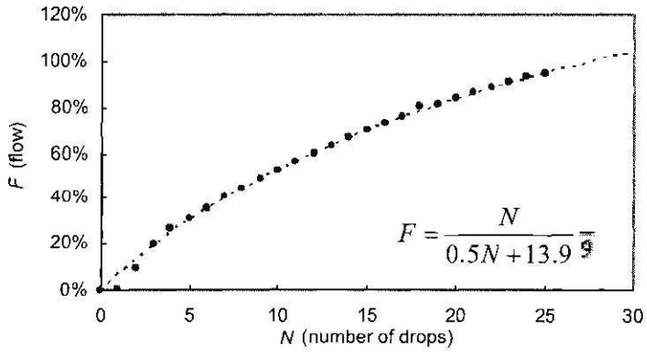

(b) Average of measured flow with drops

Figure 3.3 Flow vs. number of drops (100% Ottawa natural sand mortar). The dotted line in the lower plot is the fitted hyperbolic model

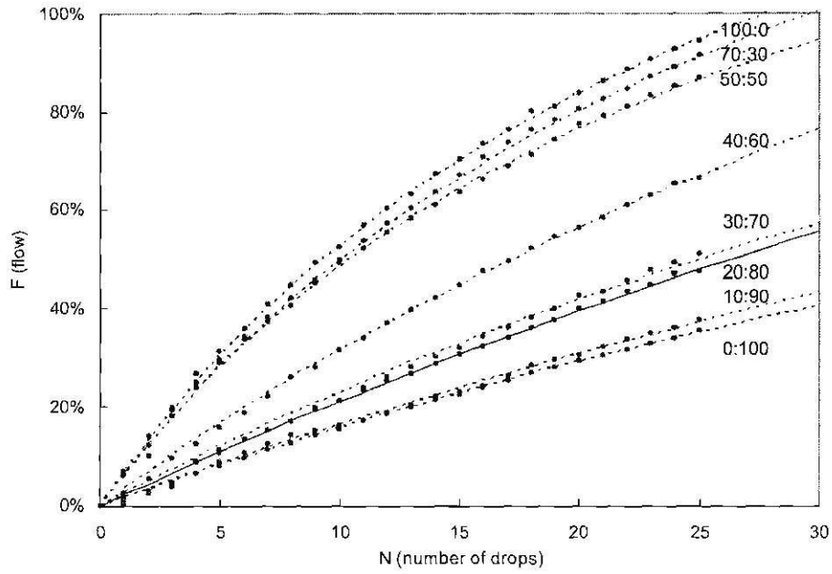

Figure 3.4 Flow curves obtained for sand mixtures (Ottawa natural sand:crushed granite sand). Dotted lines are the fitted hyperbolic model

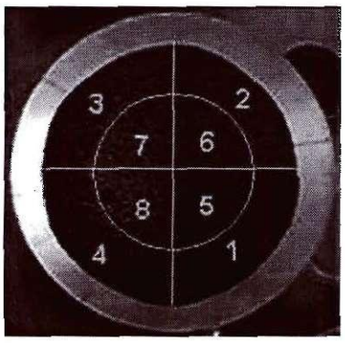

(a) Piece indices

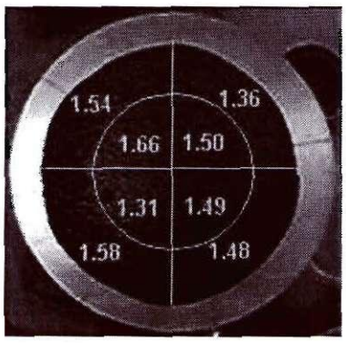

(b) Fine aggregate to paste ratio

Figure 3.5 Paste-sand segregation in flow tests after 25drops (50:50 Ottawa natural:crushed sand)

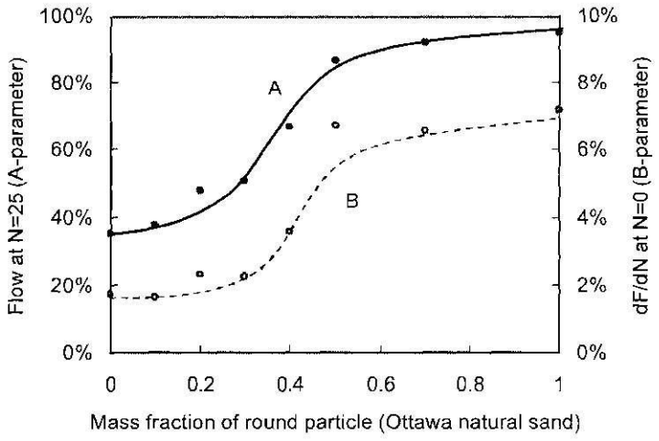

Figure 3.6 Hyperbolic model parameters vs. mass fraction of Ottawa natural sand.

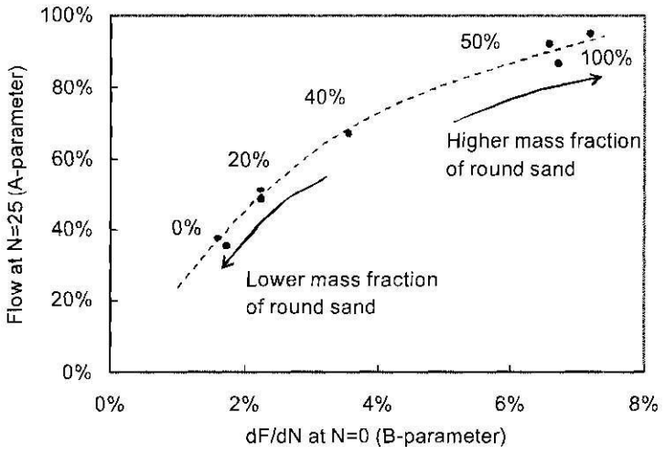

Figure 3.7 Flow at 25 drops vs. initial flow rate

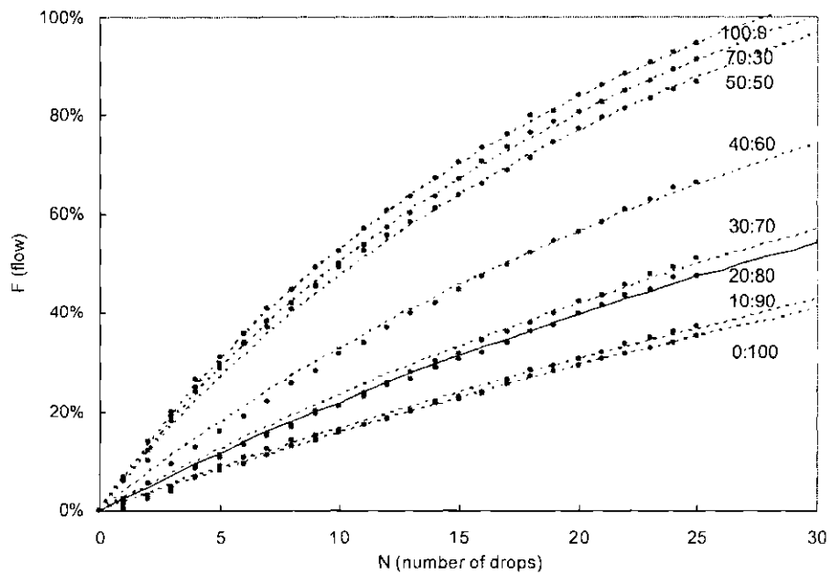

Figure 3.8 One-parameter hyperbolic model for flow at number of drops (Ottawa natural sand:crushed granite sand). Dotted lines are the fitted hyperbolic model. The asymptotic flow at an infinite number of drops is assumed 200%

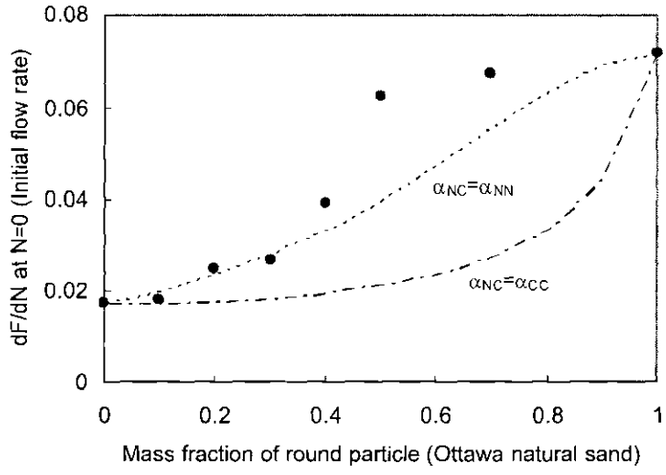

Figure 3.9 Initial flow ratio 1/b* and contact-based mixture model vs. mass fraction of round particles

Part IV. Engineering Properties of Fine Aggregates (for mortar studies)

Six different sands are selected for this study: Georgia DOT standard sand, crushed limestone sand, crushed granite sand type I, II, III (different grain size distributions), and non-Georgia natural sand. The following basic properties are measured for each material: specific gravity; maximum and minimum void ratio; roundness, sphericity and surface roughness; and angle of repose.

4.1 Grain Size Distribution

The grain size distribution is determined following sieve analysis (ASTM C136-05, see Appendix A.1 for detailed test procedure). The Georgia DOT standard sand, crushed limestone sand, crushed granite sand type I, and non-Georgia natural sand have the same gradation to study grain shape effects on mortar properties. The grain size distribution for each sand is summarized in Table 4.1 and Figure 4.1. Differences in gradation between crushed granite sand type I, II, and III are devised to explore the effect of incorporating higher fines content.

4.2 Specific Gravity

The specific gravity for each sand specimen is measured following ASTM D854-02 (Details in Appendix A.2). Results in Table 4.2 show that all the sands have very similar specific gravity.

4.3 Maximum and Minimum Void Ratios e_{max} and e_{min}

The maximum e_{max} and minimum e_{min} void ratios are determined following the ASTM D 4253–00 and ASTM D 4254–00 standards respectively. A special mold was employed for this test (Dimensions and pictures accompany the complete test procedures in Appendixes A.3 and A.4). Results are summarized in Table 4.2. Crushed limestone sand and Georgia DOT standard sand exhibit similar extreme void ratios. This suggests similar particle characteristics. Higher fine contents in crushed granite sand cause lower extreme void ratios.

4.4 Particle Shape and Surface Roughness

The roundness and sphericity of 30 sand grains are measured for different size fractions in each sand using an optical microscope (Leica MZ6 stereomicroscope, the detailed procedure can be found in Appendix A.5). Results are summarized in Table 4.3, 4.4, 4.5, and 4.6. Scanning electron microscopy (SEM, Hitachi S-800 FEG SEM) is used to evaluate the surface roughness in all particles as well as sphericity and roundness in small particles (See Figure 4.3, 4.4, and 4.5).

4.5 Angle of Repose

The angle of repose is obtained from side-view digital images of conical sand piles (The procedure is described in Appendix A.6). Results are summarized in Table 4.7, and plotted in Figure 4.6. The GDOT standard sand has the lowest friction angle f=35° which may be expected from the less angular nature of the particles. Conversely, the crushed

granite sand type III exhibits the highest friction angle f=42°. The angular shape and rough surface of the particles of crushed granite leads to higher friction angles, in agreement with published observations. Higher percentage of non-plastic fines which is smaller than 75 μm increases the friction angle of the sand.

Table 4.1 Sands and target grain size distributions

Sand Type	Passing %					
	1/2 9.5 mm	#4 4.75mm	#16 1.18mm	#50 0.300mm	#100 0.150mm	#200 0.075mm
NON-Georgia natural	100	97	60	20	5	0
Georgia DOT standard	100	98	73	15	2	0.6
Crushed Limestone/Dolomite	100	97	60	20	5	0
Crushed Granite 1	100	97	60	20	5	0
Crushed Granite 2	100	97	60	20	10	5
Crushed Granite 3	100	97	60	25	20	15

Table 4.2 Minimum and maximum void ratios and specific gravity

Sand Type	e_{min}	e_{MAX}	G_S@20°C
Crushed Granite 1	0.43	0.73	2.65
Crushed Granite 2	0.41	0.74	2.68
Crushed Granite 3	0.30	0.67	2.67
Crushed Limestone/Dolomite	0.44	0.80	2.85
Georgia DOT standard	0.51	0.80	2.67
Non Georgia natural	0.43	0.75	2.67

Table 4.3 Sphericity and roundness for Non Georgia natural sand

Sieve No.	Sphericity	Roundness	Classification
200	0.71	0.45	Subrounded
100	0.77	0.54	Rounded
50	0.62	0.34	Subangular
16	0.63	0.33	Subangular

Table 4.4 Sphericity and roundness for Georgia DOT standard sand

Sieve No.	Sphericity	Roundness	Classification
200	0.64	0.35	Subangular
100	0.66	0.33	Subangular
50	0.68	0.31	Subangular
16	0.67	0.37	Subrounded
4	0.70	0.38	Subrounded

Table 4.5 Sphericity and roundness for Crushed limestone sand

Sieve No.	Sphericity	Roundness	Classification
200	0.74	0.32	Subangular
100	0.64	0.35	Subangular
50	0.64	0.35	Subangular
16	0.56	0.26	Subangular
4	0.63	0.24	Angular

Table 4.6 Sphericity and roundness for Crushed granite sand

Sieve No.	Sphericity	Roundness	Classification
200	0.65	0.27	Subangular
100	0.63	0.30	Subangular
50	0.69	0.34	Subangular
16	0.60	0.29	Subangular
4	0.56	0.28	Subangular

Table 4.7 Angle of repose

Sand Type	F[°]
Crushed Granite 1	38
Crushed Granite 2	40
Crushed Granite 3	42
Crushed Limestone/Dolomite	37
Georgia DOT standard	36
Non Georgia natural	35

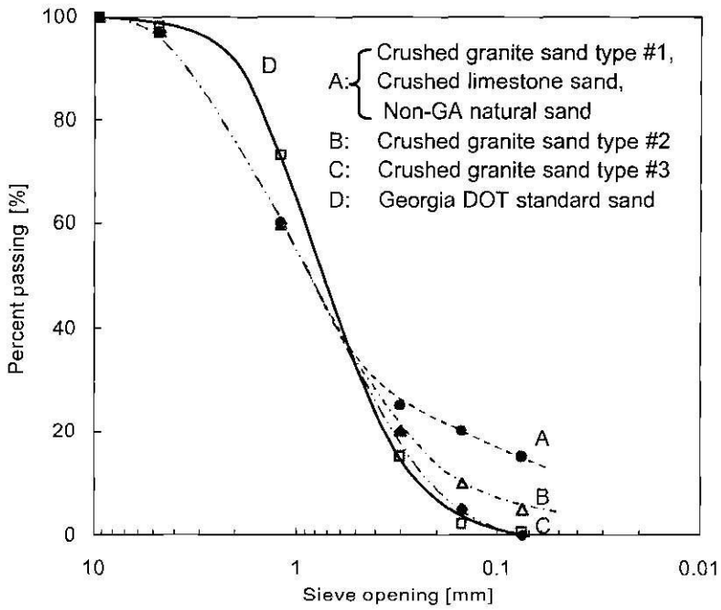

Figure 4.1 Grain size distributions of selected sands

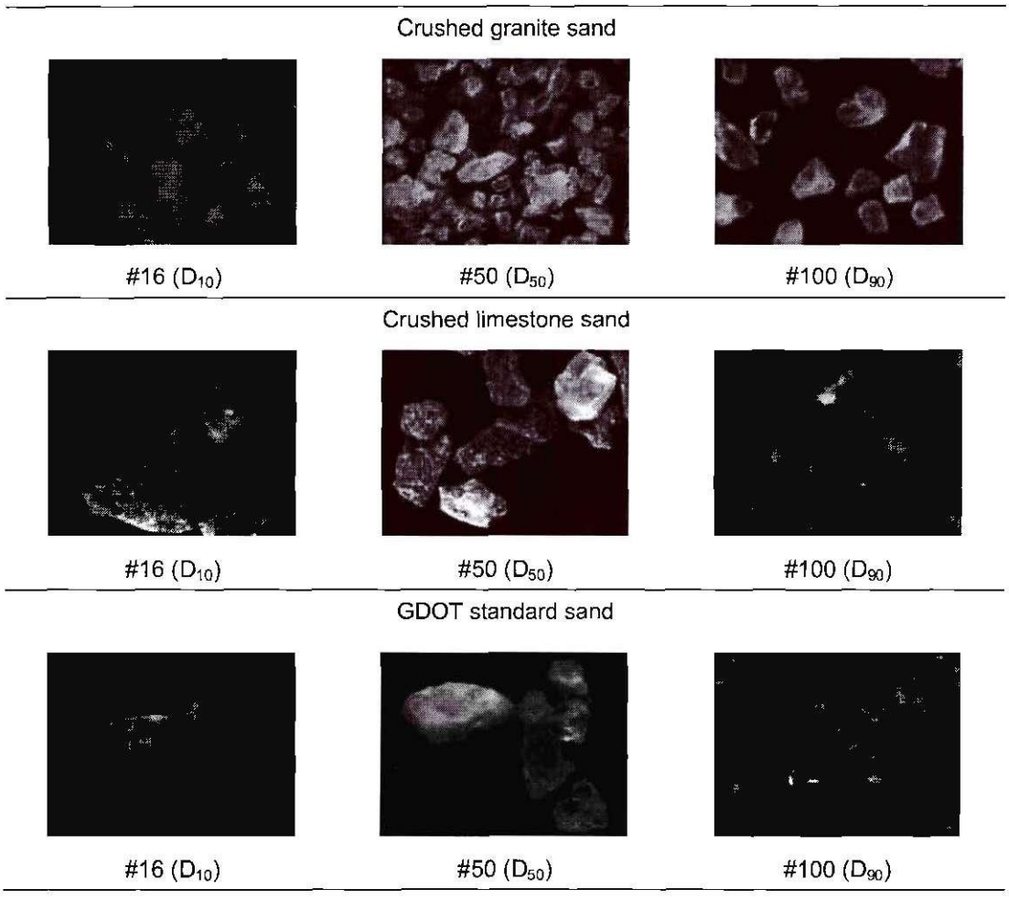

Figure 4.2 Optical microscope pictures of different-size sand particles for different selected sands

#16 (D_{10})

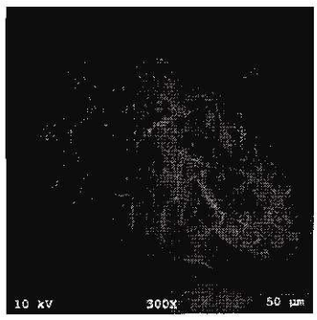

Particle scale (X300)

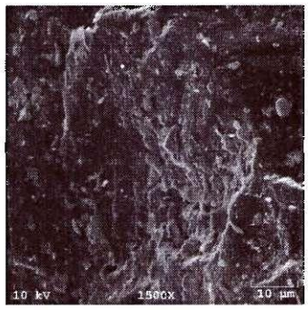

X1500

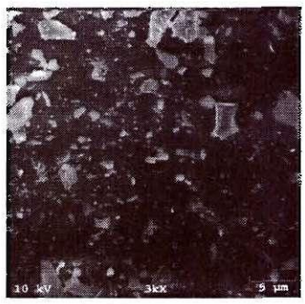

X3000

#50 (D_{50})

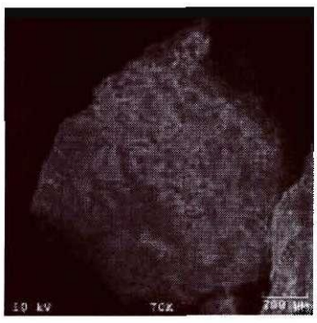

Particle scale (X70)

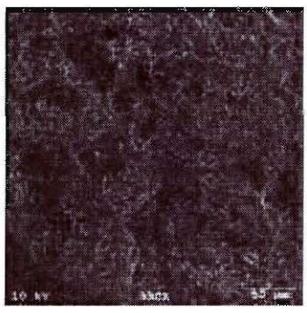

X350

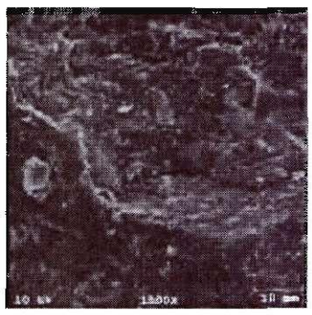

X1500

#100 (D_{90})

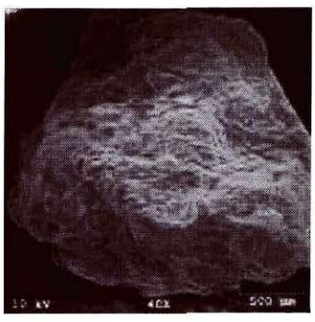

Particle scale (X40)

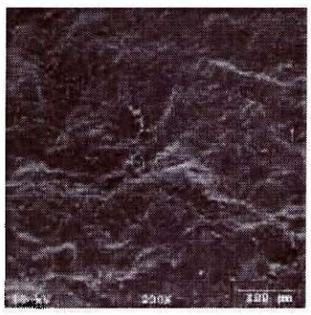

X200

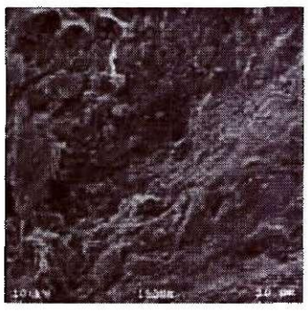

X1500

Figure 4.3 SEM pictures of Georgia natural sand particles (different size grains)

#16 (D_{10})

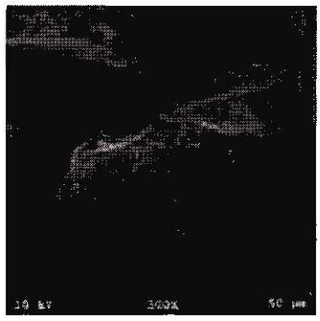

Particle scale (X300)

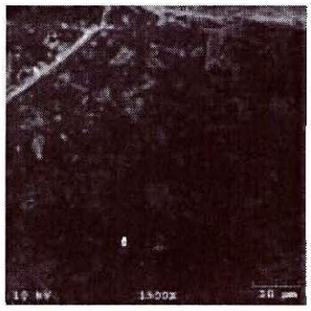

X1500

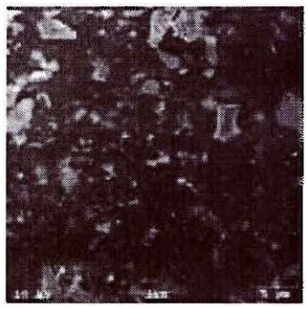

X3000

#50 (D_{50})

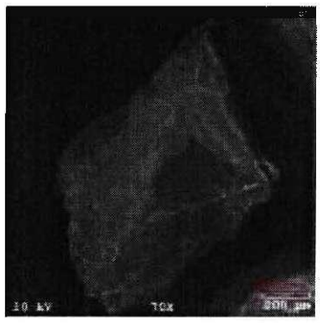

Particle scale (X70)

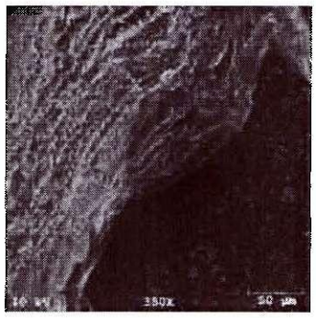

X350

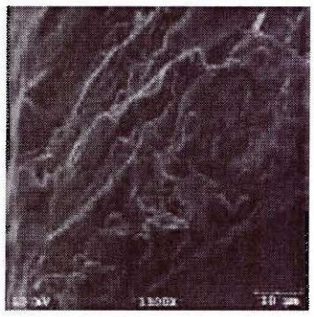

X1500

#100 (D_{90})

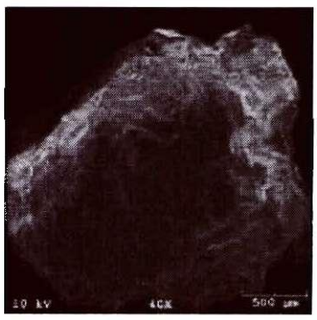

Particle scale (X40)

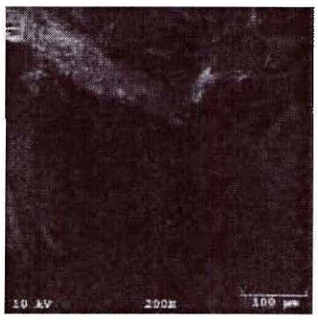

X200

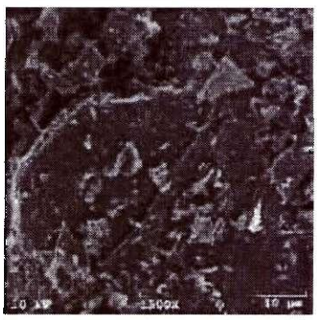

X1500

Figure 4.4 SEM pictures of crushed granite sand particles (different size grains)

#16 (D_{10})

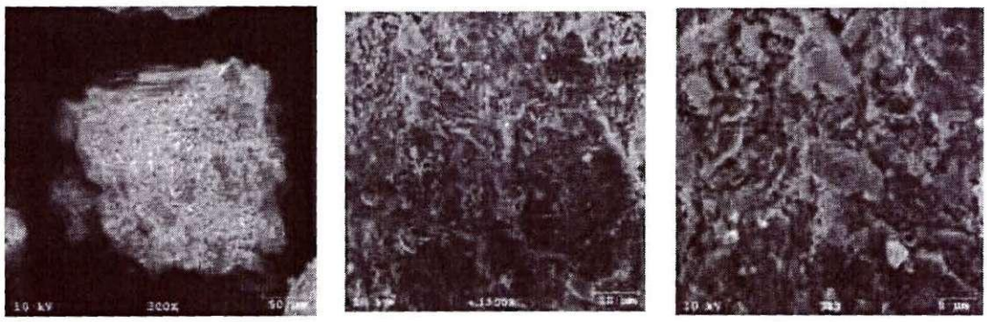

Particle scale (X300) X1500 X3000

#50 (D_{50})

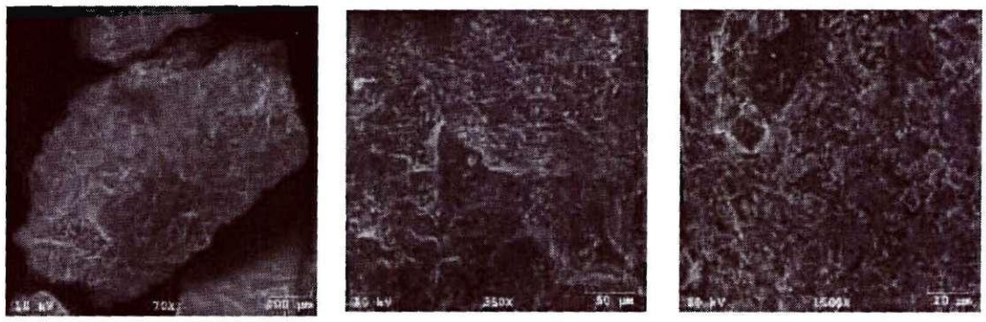

Particle scale (X70) X350 X1500

#100 (D_{90})

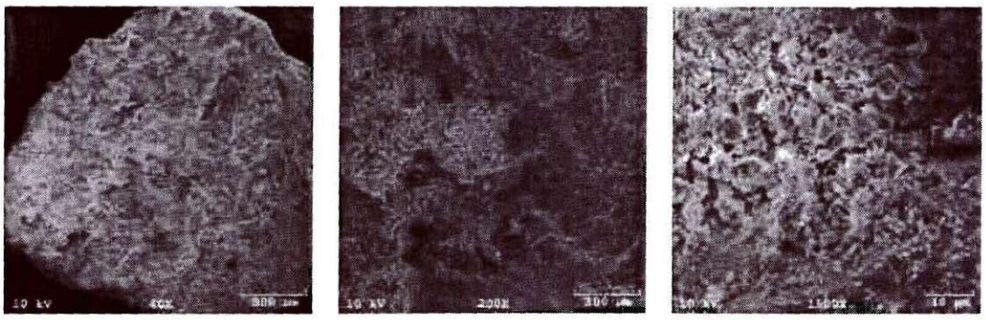

Particle scale (X40) X200 X1500

Figure 4.5 SEM pictures of crushed limestone sand particles (different size grains)

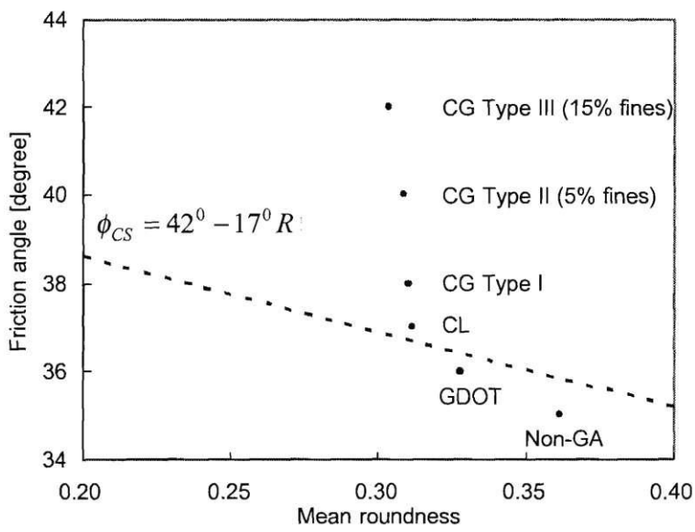

Figure 4.6 Friction angle and particle shape – Note: The presence of fines increases the friction angle. The dotted line is the mean trend for clean uniform sands (Cho et al. 2004)

Part V. Fresh and Hardened Properties of Mortar

The relationship between sand properties, mortar flow and the compressive strength required the preparation of mortars with each of the six selected sands at different water-cement and fine aggregate-cement ratios. The four different water-cement ratios are *W/C*=0.42, 0.46, 0.50 and 0.54; and the four fine aggregate-cement ratios are *FA/C*=2.00, 2.75, 3.25 and 4.00. The 96 mortars were hand-mixed (See Appendix C).

5.1 Experimental Study

Three tests are conducted for each mixture: Flow test of the fresh mortar, P-wave velocity, and unconfined compressive strength of hardened mortar cubes. Details about the test procedures are summarized in Appendices A.7, A.8 and A.9.

5.2 Test Results

The test results are presented in the following figures: Flow in Figures 5.1 through 5.6, P-wave velocity in Figures 5.7 through 5.12, and compressive strength in Figures 5.13 through 5.18.

5.3 Analysis and Discussion

P-wave velocity and compressive strength. The P-wave velocity and compressive strength of hardened concrete are positively correlated when compressive strength is below about 2000psi as shown in Figure 5.19 (see also Jones and Gatfield 1955, Orchard 1979). The type of coarse aggregate affects the P-wave velocity because the dynamic bulk stiffness of

the mineral itself is higher than that of the cement mortar (Orchard 1979); results in this study show no clear difference in the P-wave for mortars prepared with different minerals of fine aggregates.

Wetness of cement mortar flow and volume factor V_P/V_{VFA}. Photographs of the spread after 25 drops for all the mixtures are displayed in matrix form for each sand in Figures 5.20 through 5.25. "Wet flow" is herein used to designate mortars that show a continuous slurry surface. On the other hand, "dry flow" designates mortars that break and spread in granulated form. Mixtures exhibit wet flow when *W/C* is high and *FA/C* is low, i.e., the volume of cement paste is enough to coat and fill voids within the fine aggregates (Figure 5.26).

The volume of cement paste V_P and volume of voids in fine aggregates V_{VFA} can be computed from gravimetric and volumetric material properties assuming full saturation (S=100%):

$$\begin{aligned}\frac{V_P}{V_{VFA}} &= \frac{(V_C + V_W)}{e \cdot V_{FA}} \\ &= \frac{\left(\frac{W_C}{\gamma_W \cdot G_C} + \frac{W_W}{\gamma_W}\right)}{e\left(\frac{W_{FA}}{\gamma_W \cdot G_{FA}}\right)} \\ &= \frac{\frac{W_C}{\gamma_W}\left(1/G_C + W/C\right)}{e\left(\frac{W_{FA}}{\gamma_W \cdot G_{FA}}\right)} \\ &= \frac{G_{FA}\left(1/G_C + W/C\right)}{e\left(FA/C\right)}\end{aligned} \qquad (5.1)$$

where G_C is the specific gravity of cement, G_{FA} is the specific gravity of the fine aggregate, and e is the void ratio within the fine aggregates.

The two extreme sand void ratios are considered, e_{max} and e_{min}, to identify the packing condition of fine aggregates when dry flow changes wet flow. The wet or dry flow response observed in Figures 5.20 through 5.25 is plotted versus V_P/V_{VFA} in Figures 5.27 and 5.28.

The boundaries between wet and dry flow are identified at about V_P/V_{VFA}=1 to 1.2 when e_{max} is used to compute V_P/V_{VFA}, and at about V_P/V_{VFA}=1.5 to 2.5 when e_{min} is used to compute V_P/V_{VFA}. These results highlight that "wet flow" requires a volume of paste greater than the voids in fine aggregates at e_{max}: Hence, proper flow is attained when sand grains minimize touching each other.

Volume analysis of flow and compressive strength. Flow and compressive strength test results are replotted versus V_P/V_{VFA} for each mixture and sand in Figure 5.29 and 5.30. For clarity, the trends are superimposed in Figure 5.31 (flow) and Figure 5.32 (compressive strength). The peak strength is attained at a value of V_P/V_{VFA} higher than the value of V_P/V_{VFA} at the minimum flow. Hence, peak strength develops in specimens that exhibit wet flow. The positive correlation between increased flow and increased strength takes place between a relatively narrow range of V_P/V_{VFA} only. These observations are highlighted in Figure 5.33.

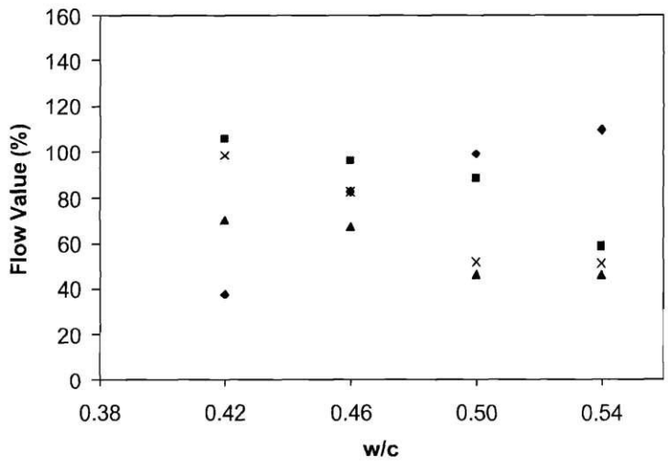

Figure 5.1 Flow test results for crushed granite sand type I

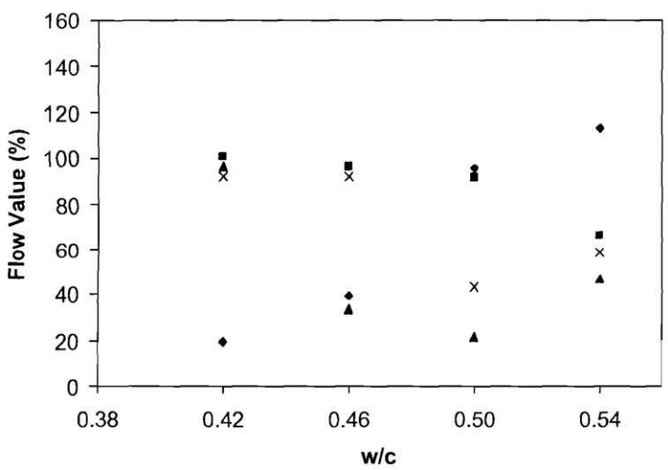

Figure 5.2 Flow test results for crushed granite sand type II

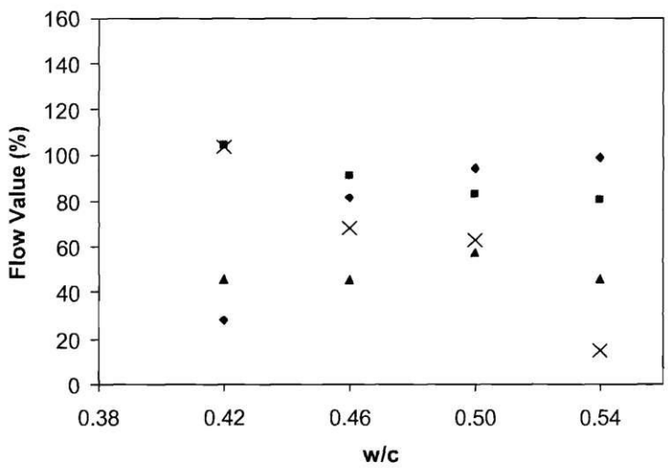

Figure 5.3 Flow test results for crushed granite sand type III

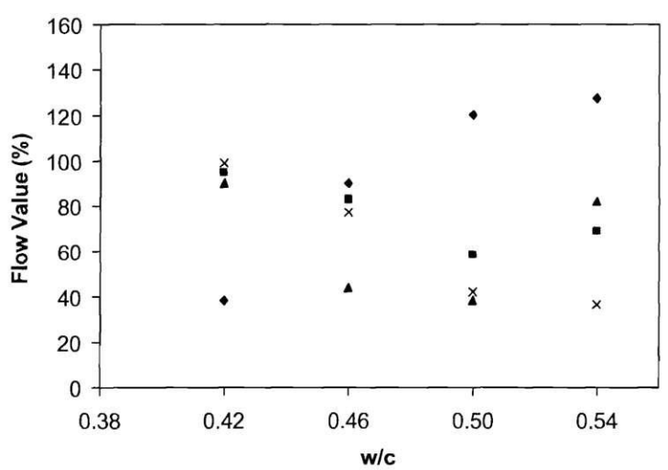

Figure 5.4 Flow test results for crushed limestone sand

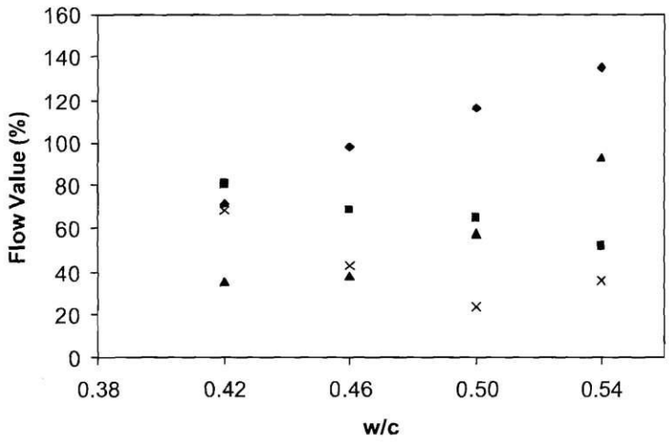

Figure 5.5 Flow test results for Non-GA natural sand

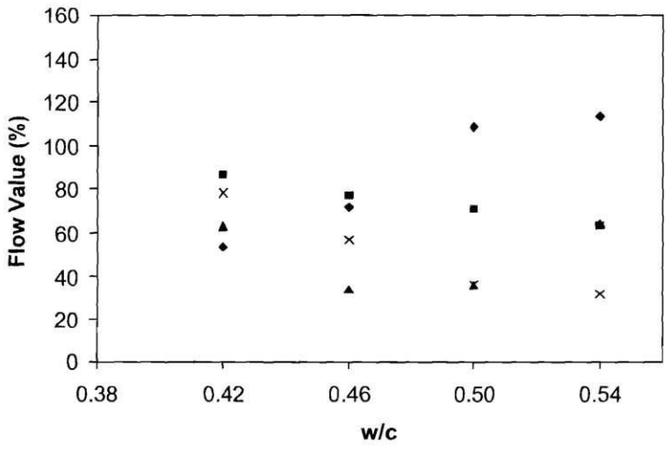

Figure 5.6 Flow test results for Georgia DOT standard sand

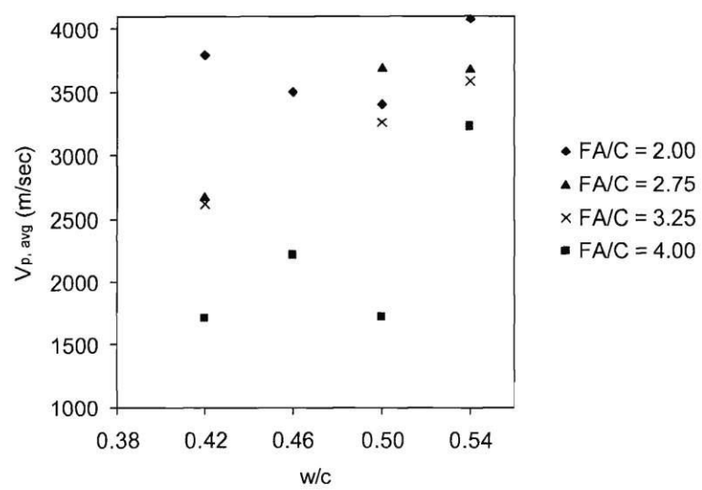

Figure 5.7 P-wave velocity for mortar made of crushed granite sand type I

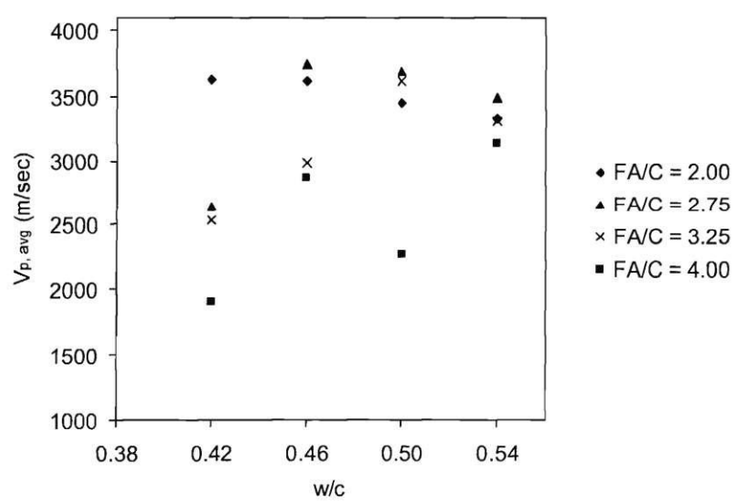

Figure 5.8 P-wave velocity for mortar made of crushed granite sand type II

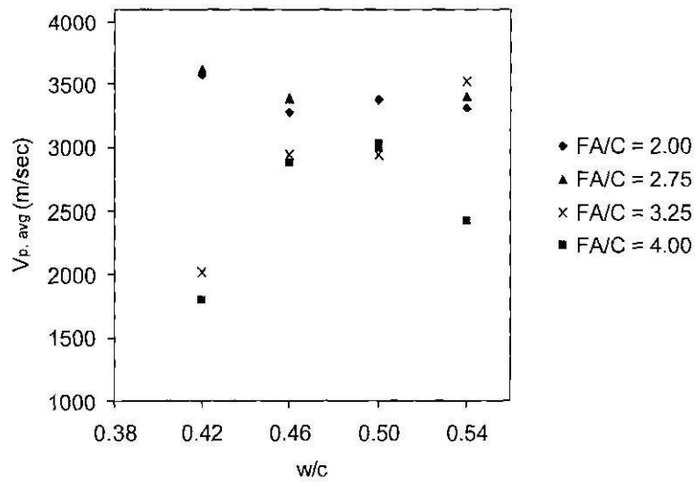

Figure 5.9 P-wave velocity for mortar made of crushed granite sand type III

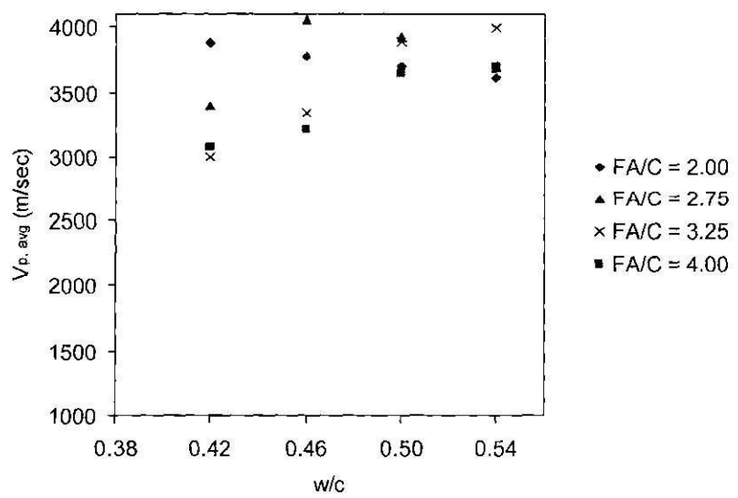

Figure 5.10 P-wave velocity for mortar made of crushed limestone sand

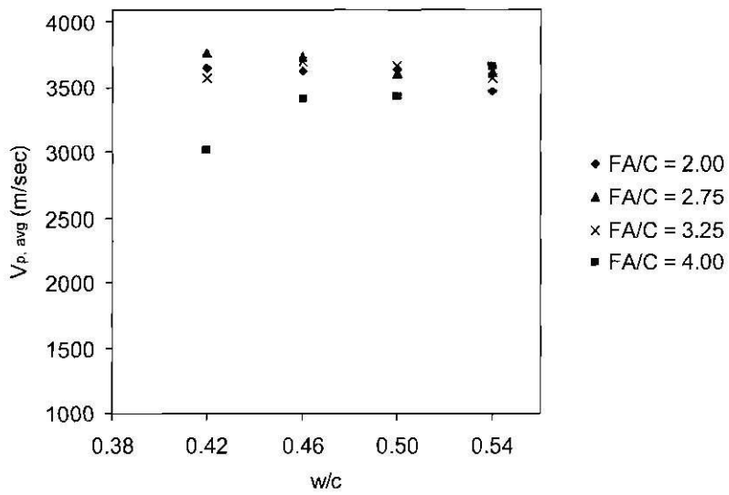

Figure 5.11 P-wave velocity for mortar made of non-Georgia natural sand

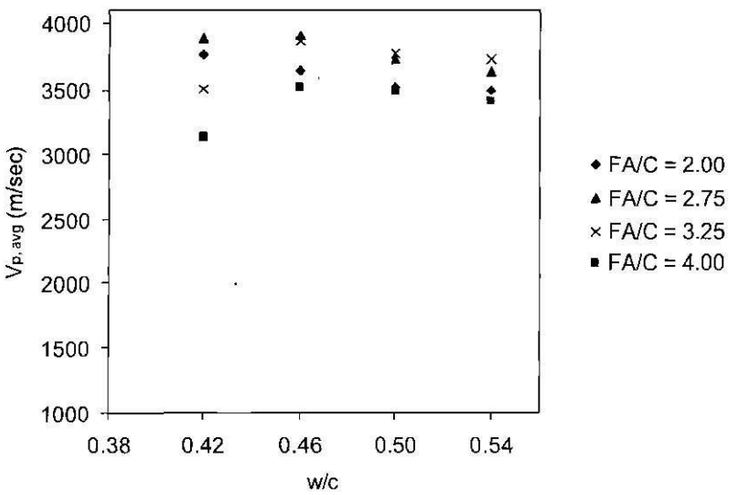

Figure 5.12 P-wave velocity for mortar made of GDOT standard sand

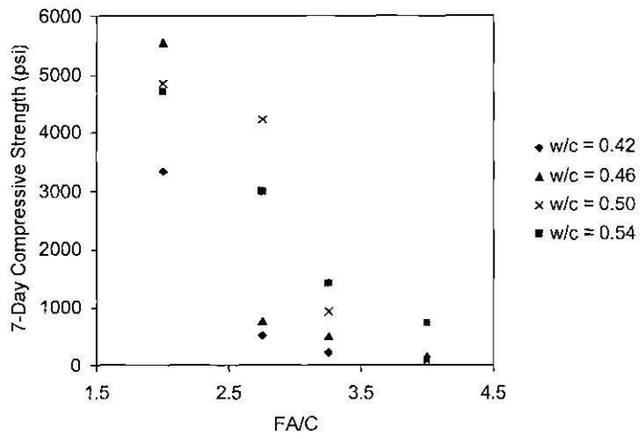

Figure 5.13 Seven day peak compressive strength for mortar made of crushed granite sand type I

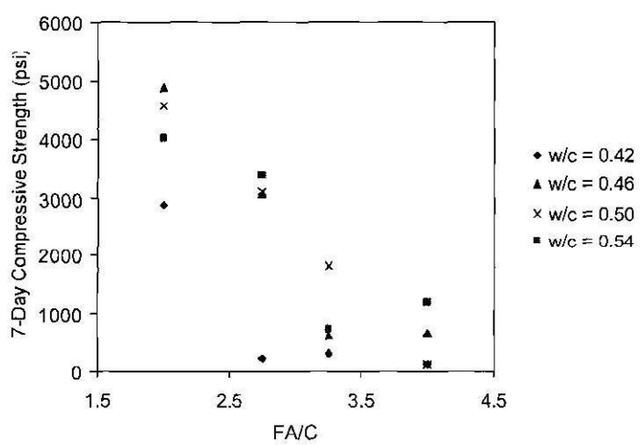

Figure 5.14 Seven day peak compressive strength for mortar made of crushed granite sand type II

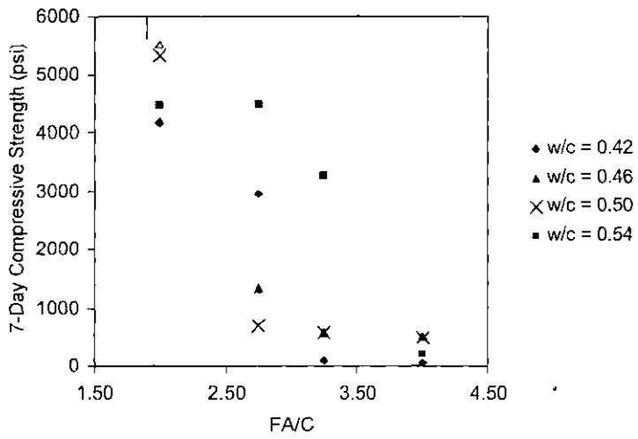

Figure 5.15 Seven day peak compressive strength for mortar made of crushed granite sand type III. Note: Cubes that did not fail at the maximum equipment capacity of 22010 lbs are represented as open symbols

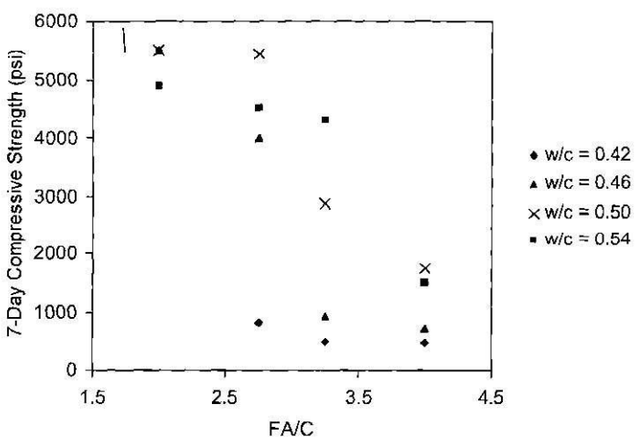

Figure 5.16 Seven day peak compressive strength for mortar made of crushed limestone sand. Note: Cubes that did not fail at the maximum equipment capacity of 22010 lbs are represented as open symbols

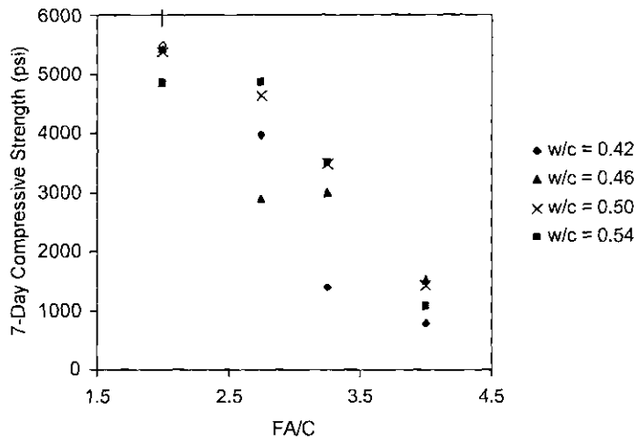

Figure 5.17 Seven day peak compressive strength for mortar made of non-Georgia natural sand. Note: Cubes that did not fail at the maximum equipment capacity of 22010 lbs are represented as open symbols

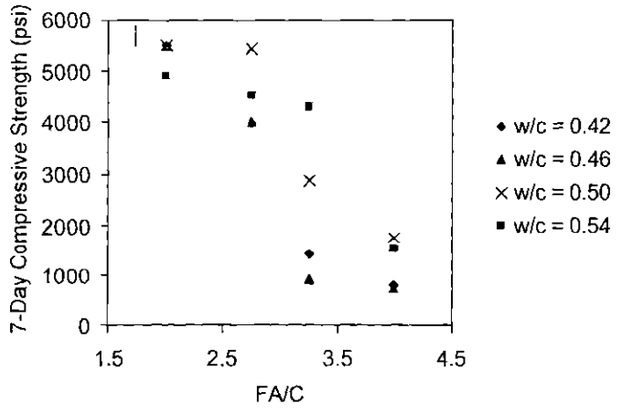

Figure 5.18 Seven day peak compressive strength for mortar made of GDOT standard sand: . Note: Cubes that did not fail at the maximum equipment capacity of 22010 lbs are represented as open symbols

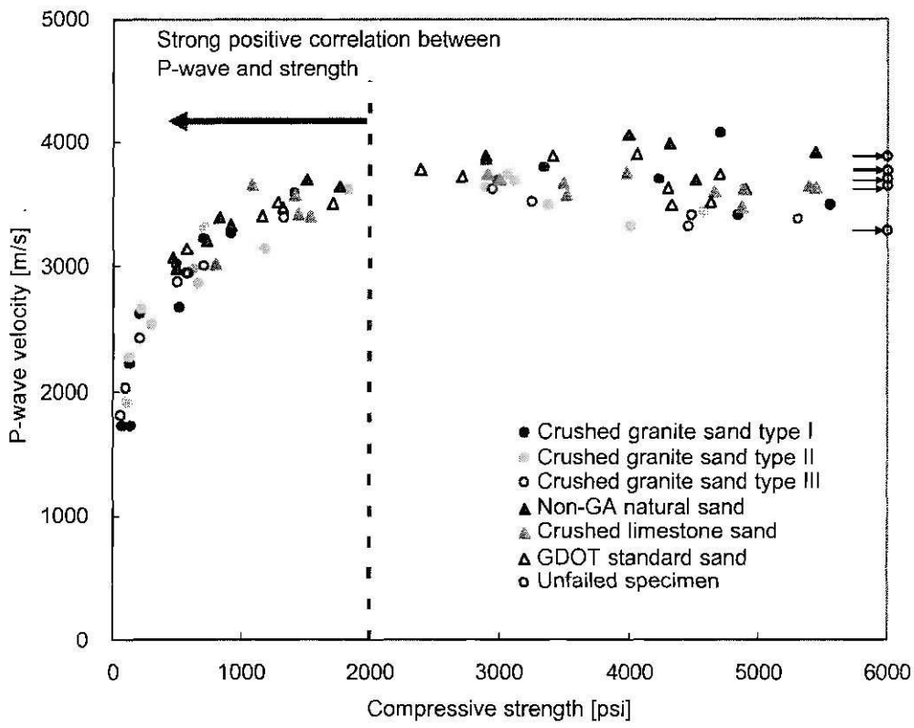

Figure 5.19 Compressive strength versus P-wave velocity: Seven day hardened cement mortars

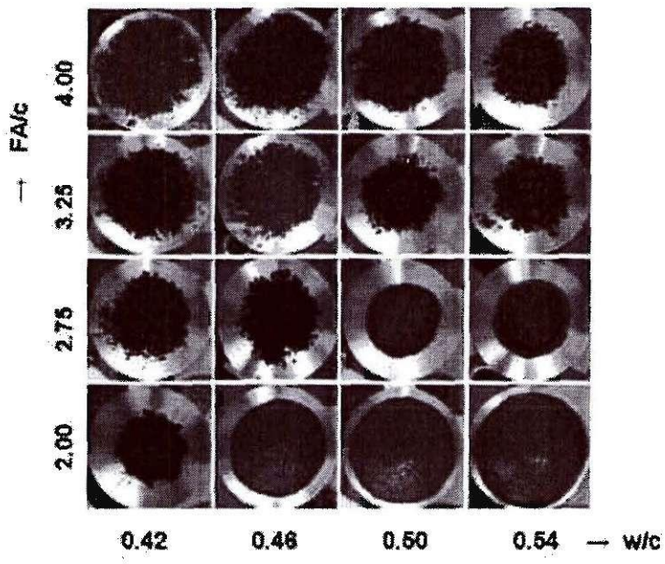

Figure 5.20 Pictures of flow at 25 drops. All mortars are prepared with crushed granite sand type I

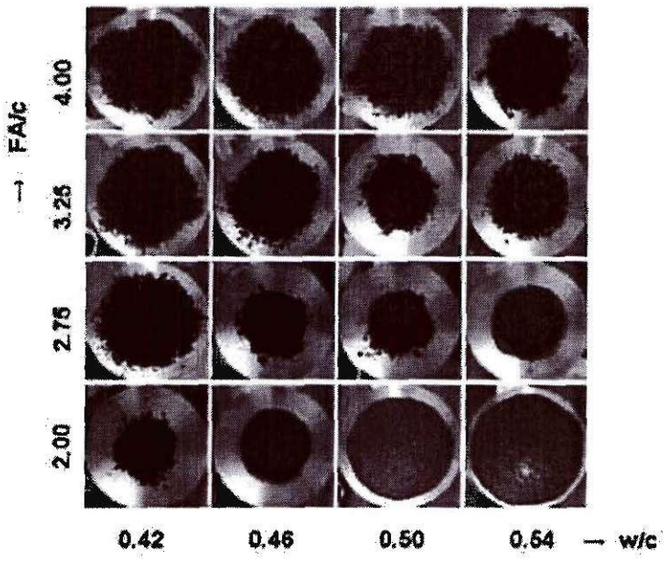

Figure 5.21 Pictures of flow at 25 drops. All mortars are prepared with crushed granite sand type II

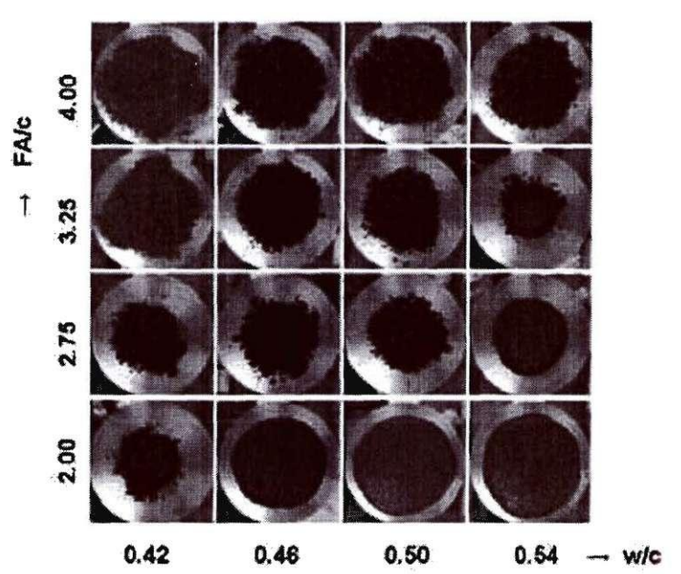

Figure 5.22 Pictures of flow at 25 drops. All mortars are prepared with crushed granite sand type III

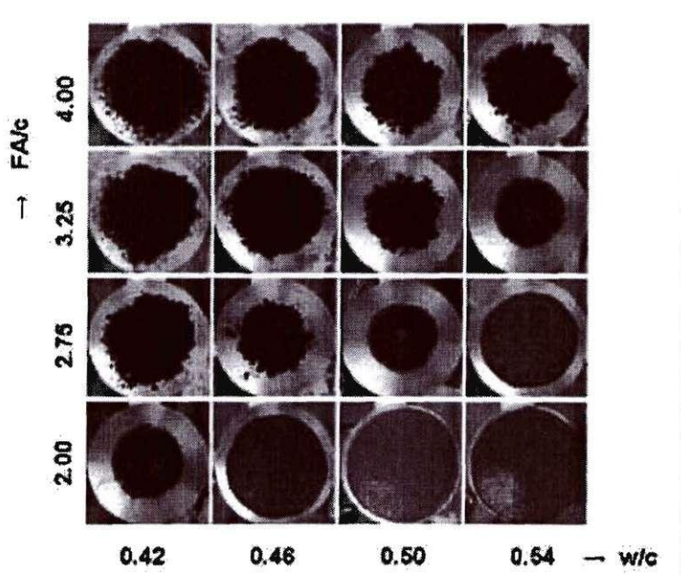

Figure 5.23 Pictures of flow at 25 drops. All mortars are prepared with crushed limestone sand

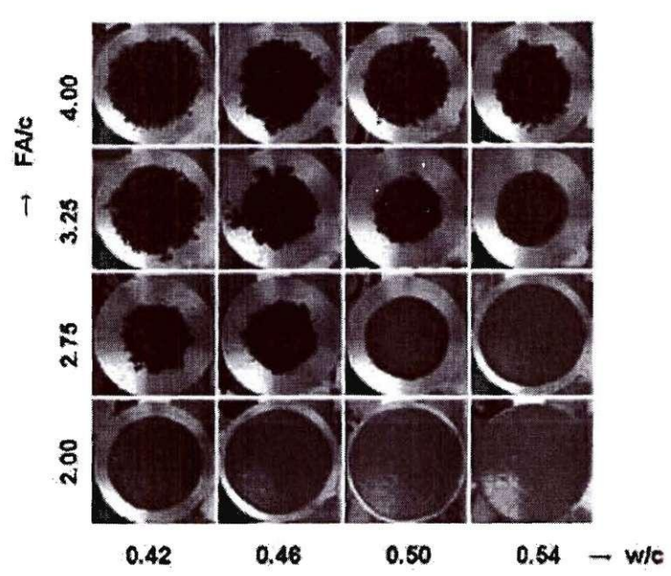

Figure 5.24 Pictures of flow at 25 drops. All mortars are prepared with non-Georgia natural sand

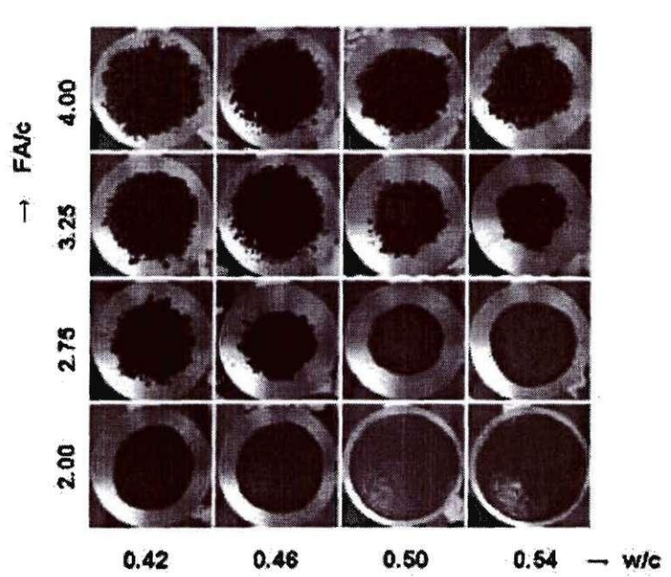

Figure 5.25 Pictures of flow at 25 drops. All mortars are prepared with Georgia DOT standard sand

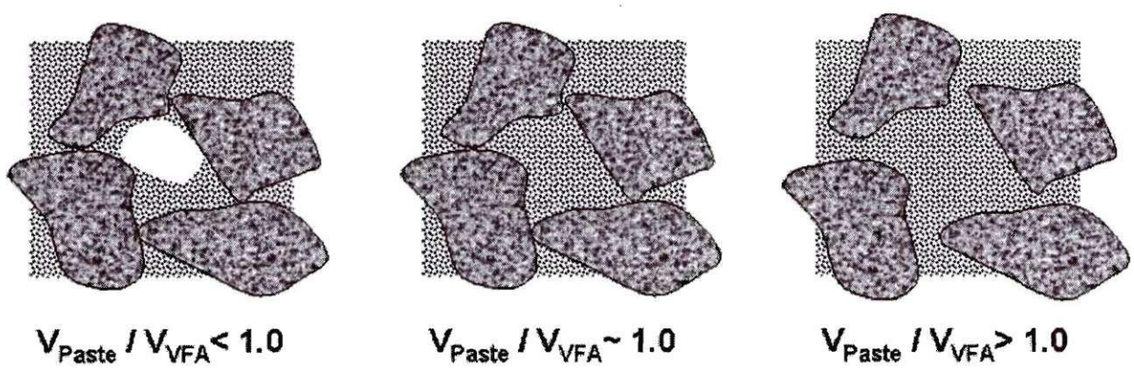

Figure 5.26 Volumetric relationship between cement paste and voids in fine aggregates: $V_{VFA}=V_{total}-V_{FA}$=(Volume of mortar without fine aggregates)

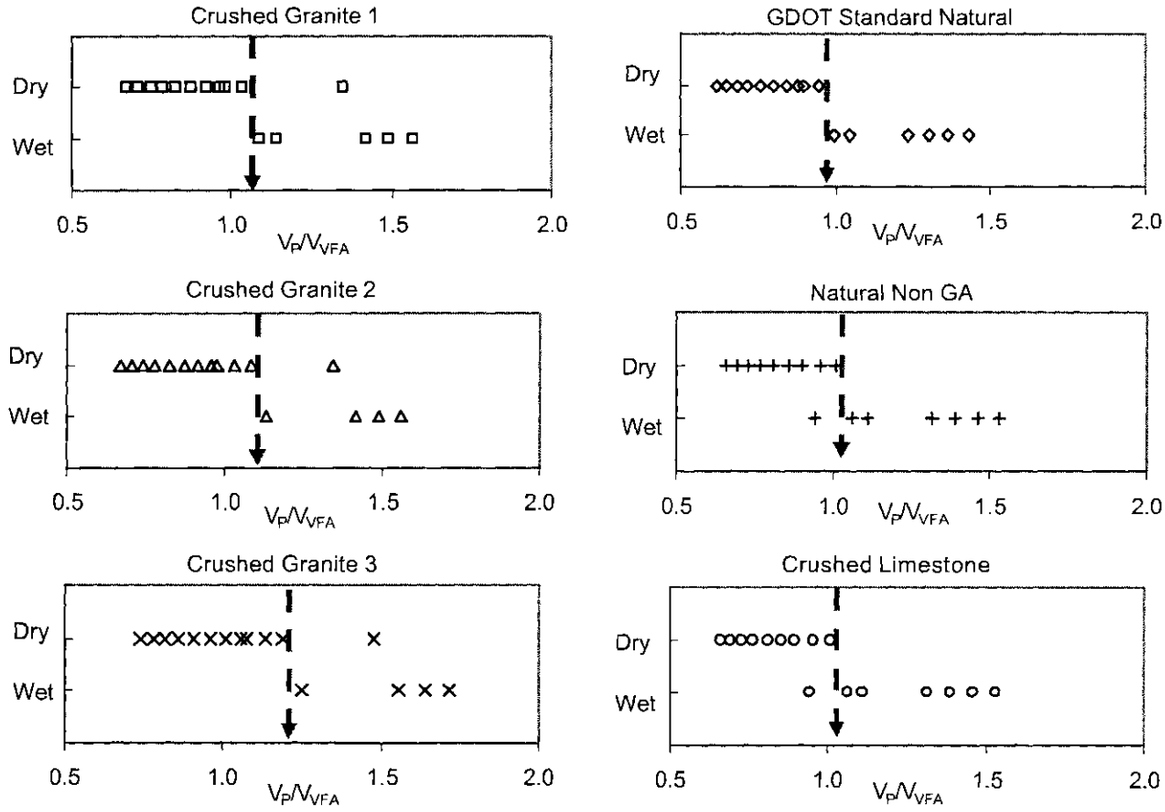

$$\frac{V_P}{V_{VFA}} = \frac{G_{FA}\left(1/G_C + W/C\right)}{e_{\max}\left(FA/C\right)}$$

Figure 5.27 "Wetness" from flow pictures vs. relative V_P/V_{VFA} computed with e_{max}. The arrows indicate the boundary between "dry flow" and "wet flow"

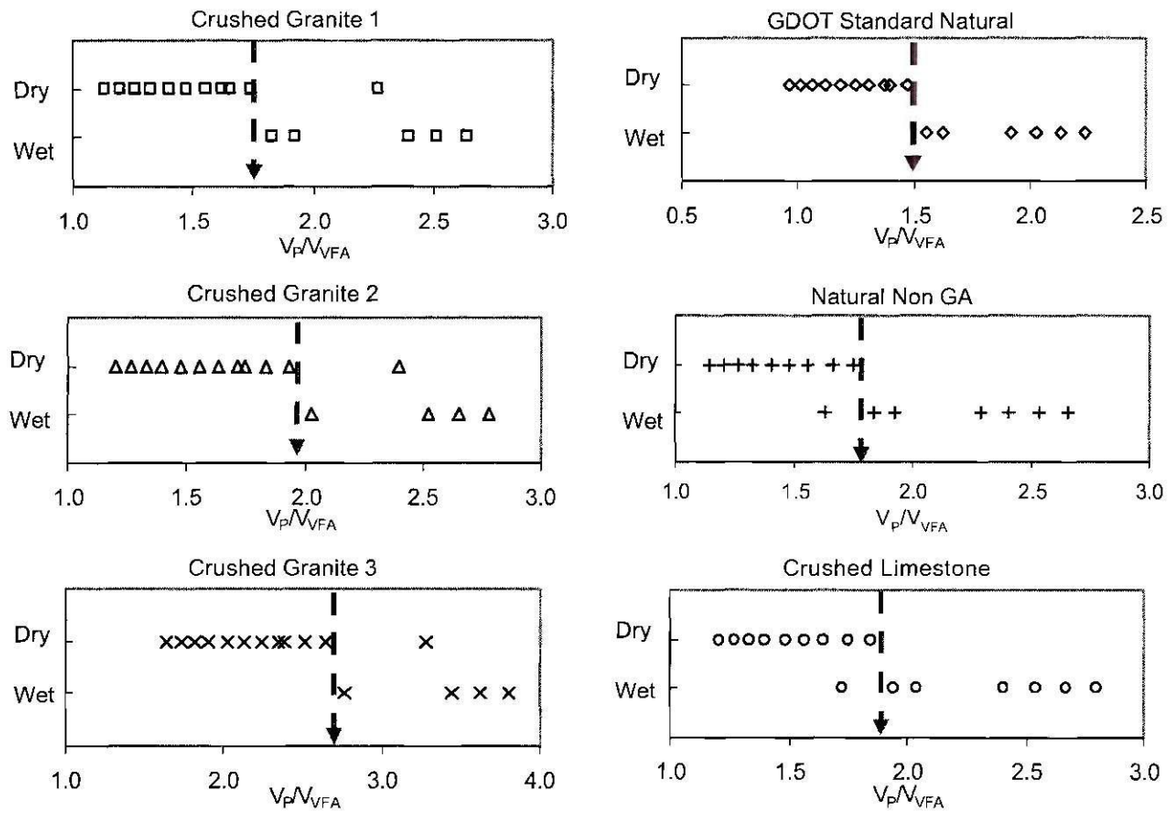

$$\frac{V_P}{V_{VFA}} = \frac{G_{FA}\left(1/G_C + W/C\right)}{e_{\min}\left(FA/C\right)}$$

Figure 5.28 "Wetness" from flow pictures vs. relative V_P/V_{VFA} computed with e_{min}. The arrows indicate the boundary between "dry flow" and "wet flow"

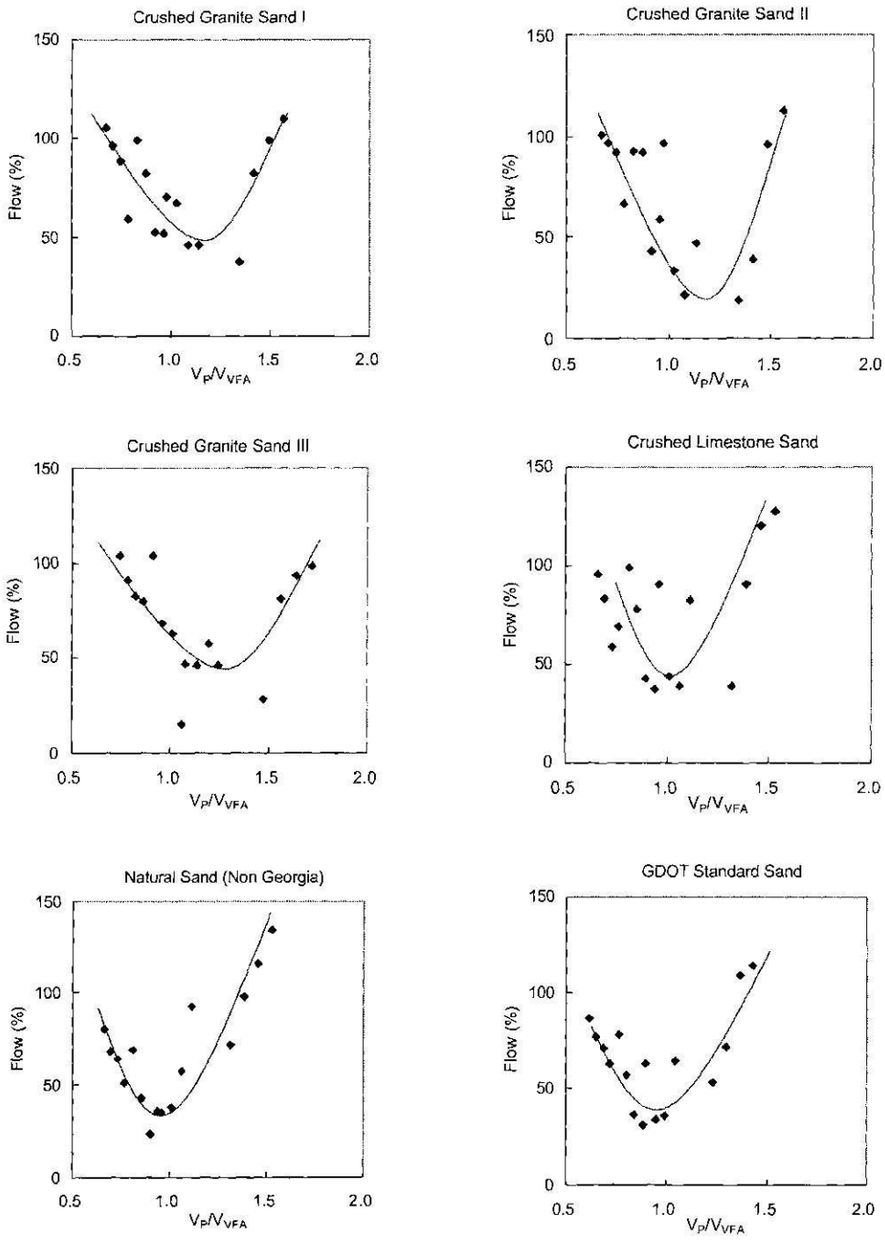

Figure 5.29 Flow vs. volume factor V_P/V_{VFA}

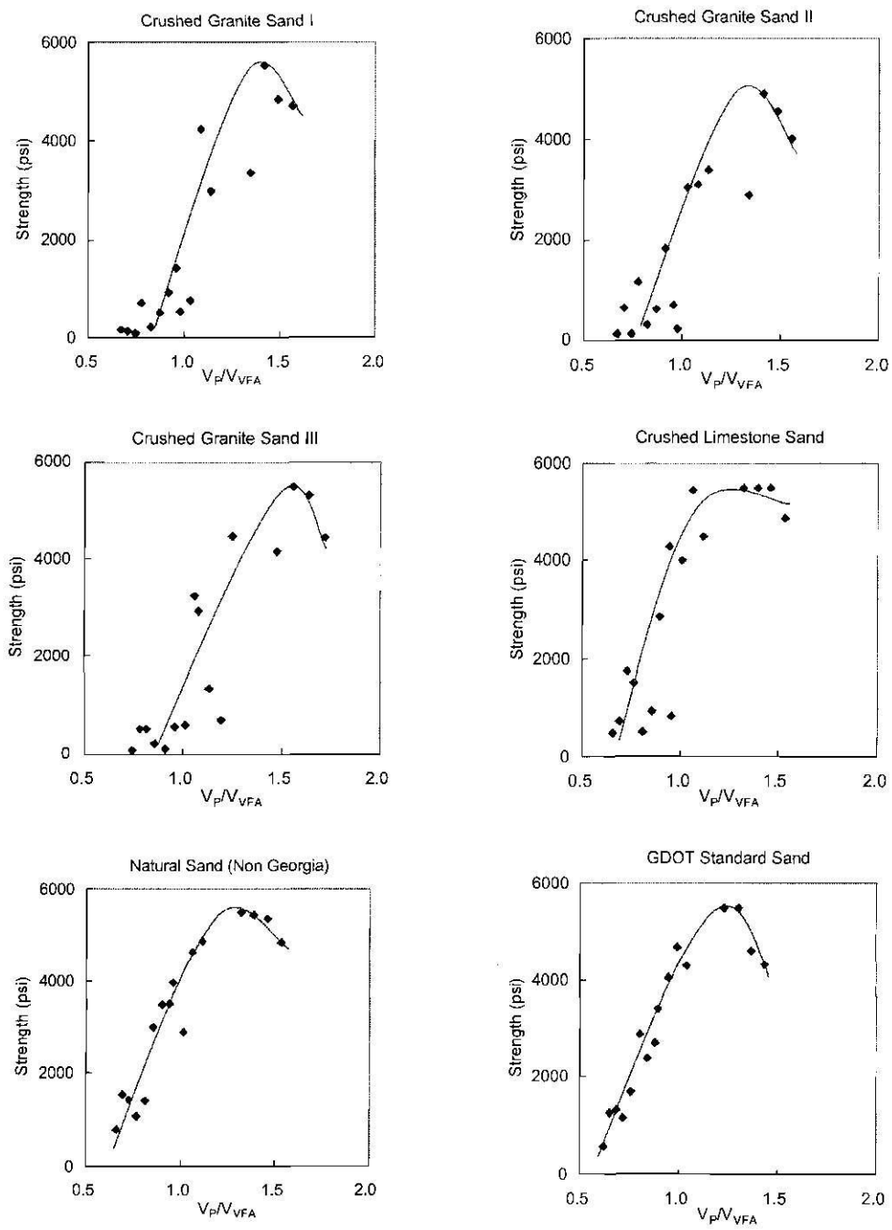

Figure 5.30 Compressive strength vs. volume factor V_P/V_{VFA}

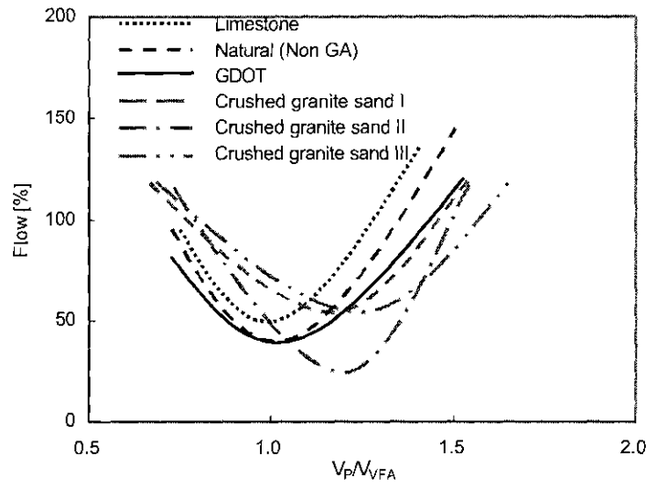

Figure 5.31 Flow vs. volume factor for all sands and mixtures

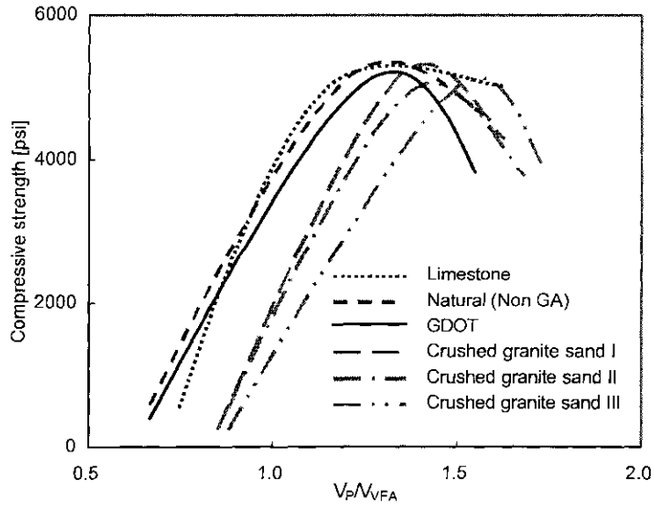

Figure 5.32 Compressive strength vs. volume factor for all sands and mixtures

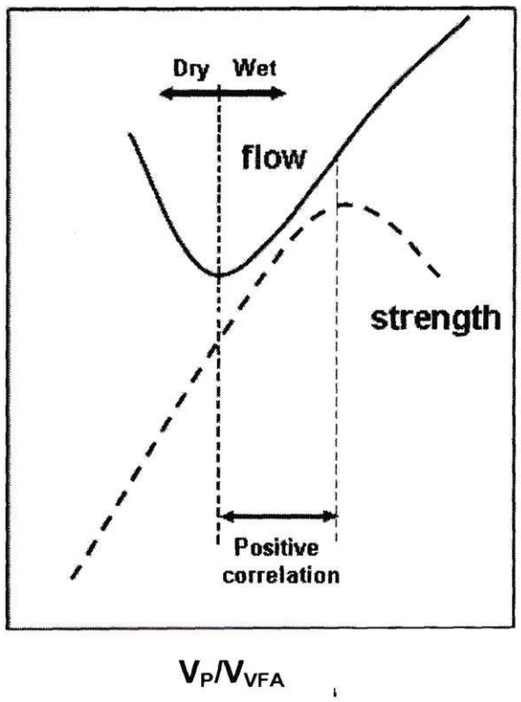

Figure 5.33 Schematic diagram of flow and compressive strength vs. volume factor V_P/V_{VFA}

VI. Conclusions

We implemented a comprehensive experimental study of the flow test, and evaluated its ability to assess the effect of sand characteristics on cement mortar. We tested eight different natural and crushed sands at different water-to-cement and fine aggregate-to-cement ratios. The following conclusions can be drawn from this study:

- There is a hyperbolic nonlinear relationship between flow F and the number of drops N. A single parameter is needed to characterize the flow-drop trend, i.e.: the initial flow rate.
- Round particles begin exerting a strong effect on flow when the mass fraction of round particles exceeds 30-50%. The presence of round particles in the mortar is more effective in promoting flow than the crushed particles in hindering it.
- Crushed aggregates exhibit significant surface roughness at a scale of about $0.1D$ where D is the particle diameter.
- Crushed limestone sand and the Georgia DOT standard sand exhibit similar particle shapes, extreme void ratios, and angles of repose. Such similarities explain the resemblance in compressive strength and flow shown by the mortars prepared with these two sands.
- The P-wave velocity and compressive strength of hardened mortar are positively correlated when the compressive strength is below 2000 psi, regardless of the type of sand. The P-wave velocity remains constant when the strength exceeds 2000 psi.
- Mortar flow becomes "wet" when the volume of paste is greater than the volume of voids within the fine aggregate at a void ratio between e_{max} and $1.1\ e_{max}$.

- The peak strength is attained at a value of V_P/V_{VFA} higher than the value of V_P/V_{VFA} at the minimum flow. Hence, peak strength develops in specimens that exhibit wet flow.
- Peak strength and flow are positively correlated within the relatively narrow range of the volume factor V_P/V_{VFA} between the value of V_P/V_{VFA} corresponding to minimum flow and the value of V_P/V_{VFA} corresponding to peak strength.
- Good quality mortar can be prepared with any of natural and crushed sands tested here (even with 15% of fines). However, the optimal mix varies with the type of sand.

References:

ASTM C 109 "Standard Test Method for Compressive Strength of Hydraulic Cement Mortars." *American Society for Testing and Materials*

ASTM C136-05 "Standard Test Method for Sieve Analysis of Fine and Coarse Aggregates." *American Society for Testing and Materials*

ASTM C1437-01 "Standard Test Method for Flow of Hydraulic Cement Mortar." *American Society for Testing and Materials*

ASTM D854-02 "Standard Test Methods for Specific Gravity of Soil Solids by Water Pycnometer." *American Society for Testing and Materials*

ASTM D 4253–00 "Standard Test Methods for Maximum Index Density and Unit Weight of Soils Using a Vibratory Table." *American Society for Testing and Materials*

ASTM D 4254–00 "Standard Test Methods for Minimum Index Density and Unit Weight of Soils and Calculation of Relative Density." *American Society for Testing and Materials*

Banfill, P. F. G. (1994). "Rheological Methods for Assessing the Flow Properties of Mortar and Related Materials." *Construction and Building Materials*, 8(1),43-50.

Bartos, P., (1992) *Fresh Concrete: Properties and Tests*, Elsevier

Bodenlos, K. D., and Fowler, D. W. (2003). "Qualification of Concrete Workability by Means of the Vibrating Slope Apparatus." *ICAR 105-2*, International Center for Aggregates Research The University of Texas at Austin.

Brookbanks, P. (1989). *Properties of Fresh Concrete*, Building Research Establishment,

Garston, Watford, England.

Cho, G.-C., Dodds, J. and Santamarina, J.C. (2004) "Particle Shape Effects on Packing Density, Stiffness and Strength," *Internal Report*, Georgia Institute of Technology

Collins, R. R., Slaughter, P., and Cown, R. M. "Utilization of Fines in Concrete." *ICAR*, The University of Texas at Austin.

Diamond, C.R., and Bloomer , S.J., (1977) "A Consideration of the DIN Flow Table," *Concrete* (London), Vol. 11, No. 12, pp. 29-30

DIN 1048, (1972) "Testing Methods of Concrete," *Deutsches Institut für Normung* e.V., Berlin, Clause 312

Dodds, J. (2003). *Particle Shape and Stiffness Effects on Soil Behavior,* M.S thesis Georgia Institute of Technology, Atlanta.

EN12350-5: 2000, (2000) "Testing fresh concrete – Part 5: Flow table test," *European Committee for Standardization.*

Ferraris, C. (1999). "Measurement of the rheological properties of high performance concrete; State of the art report." *Journal of Research of the National Institute of Standards and Technology*, Vol. 104, No. 5, pp. 461-478.

Ferraris, C., and de Larrard, F. (1998). "Modified slump test to measure rheological parameters of fresh concrete." *Cement Concrete and Aggregates*, Vol. 20, No. 2, pp. 241-247.

Ferraris, C., and Gaidis, J. (1992). "Connection Between the Rheology of Concrete and Rheology of Cement Paste." *ACI Materials Journal*, Vol. 89, No. 4, pp. 388-393.

Flatt, R., Martys, N., and Bergstrom, L. (2004). "The rheology of cementitious materials."

MRS Bulletin, Vol. 29, No. 5, pp. 314-318.

Fowler, D. W., and Constantino, C. A. (1997) "International Research on Fines in Concrete." *ICAR 5th Annual Symposium Proceedings*, The University of Texas at Austin, C2-4-1.

Jackson, N. M., and Brown, R. H. (1996). "Use of Higher Fines Contents in Portland Cement Concrete." *ICAR symposium*, Atlanta.

Jones, R. and Gatfield, E.N., (1955) Testing concrete by an ultrasonic pulse technique, *Road Research Technical Paper* No. 34

Kaplan, M. F. (1959). "Flexural and Compressive Strength of Concrete as Affected by the Properties of Coarse Aggregates." *American Concrete Institute*, 55, pp.1193-1208.

Kaplan, M.F., (1959) "The effect of age and water/cement ratio upon the relation between ultrasonic pulse velocity and compressive strength of concrete," *Magazine of Concrete Research*, Vol. 11, No. 32

Koehler, E.P. and Fowler, D.W., (2003) Summary of Concrete Workability Test Methods, *ICAR Report* 105.1, International Center for Aggregates Research, the University of Texas at Austin

Mor, A., and Ravina, D., (1986) "The DIN Flow Table: A Complement to the Slump Test for High Slump Concrete," *Concrete International*, Vol. 8, No. 12, pp. 53-56

NSSGA (National stone, sand and gravel association), *50 Fascinating Facts about Stone, Sand & Gravel*, Arlington, VA, http://www.nssga.org/pdf/50facts.pdf.

Orchard, D.F., (1979) *Concrete technology*, Applied Science Publisher Ltd., London

Plawsky, J.L., Jovanovic, S., Littman, H., Hover, K.C., Gerolimatos, S., and Douglas, K.,

(2003) "Exploring the effect of dry premixing of sand and cement on the mechanical properties of mortar," *Cement and Concrete Research*, Vol. 33, pp. 255-264

Quiroga, P., and Fowler, D. (2004) "Chemical Admixtures and Supplementary Cementing Materials in Concrete with High Microfines." *ICAR.*

Quiroga, P., and Fowler, D. (2003) "The Effects of Aggregates Characteristics on the Performance of Portland Cement Concrete." *ICAR 104-1F*, International Center for Aggregates Research.

Rahman, M., and Nehdi, M. (2003). "Effect of geometry, gap, and surface friction of test accessory on measured rheological properties of cement paste." *ACI Materials Journal*, Vol. 100, No. 4, pp. 331-339.

Roy, D.M. and Idorn, G.M., (1993) *Concrete Microstructure*, Strategic Highway Research Program Report, SHPR-C-340, National Academy of Sciences

Santamarina, J. C., and Cho, G. C. (2004) "Soil behaviour: The role of particle shape." *Skempton Conference*, London.

Schiller, B., and Ellerbrock, H. G. (1992). "The Grinding and Properties of Cement with Several Main Constituents." *Zement-Kalk-Gips*, Vol. 45, No. 7, pp. 325-334.

Schmidt, M. (1992a). "Cement with Interground Additives - Capabilities and Environmental Relief, Part 1." *Zement-Kalk-Gips*, Vol. 45, No. 7, pp. 64-69.

Schmidt, M. (1992b). "Cement with Interground Additives - Capabilities and Environmental Relief, Part 2." *Zement-Kalk-Gips*, Vol. 45, No. 6, pp. 296-301.

Tattersall, G.H. and Banfill, P.F.G. (1983) *The Rheology of Fresh Concrete*, Pitman

Advanced Publishing Program

Tattersall, G.H., (1991) *Workability and Quality Control of Concrete*, E&FN Spon, London

Williams, D. A., Saak, A. W., and Jennings, H. M. (1999). "The influence of mixing on the rheology of fresh cement paste." *Cement and Concrete Research*, Vol. 29, No. 9, pp.1491-1496.

Yang, M., and Jennings, H. M. (1995). "Influences of Mixing Methods on the Microstructure and Rheological Behavior of Cement Paste." *Advanced Cement Based Materials*, Vol. 2, No. 2, pp. 70-78.

Zollinger, D. G., and Sarkar, S. (2001). "Framework for Development of a Classification Procedure for Use of Aggregate Fines in Concrete." *ICAR 101-2F.*

Appendix A. Test Procedures

A.1 Sieve Analysis for Fine Aggregates (ASTM C136-05)

1. Order the sieves from large opening to small opening and place them in the mechanic shaker
2. Weight 300g of dry fine aggregate
3. Place the aggregate in the upper sieve and place the lid
4. Shake for 3 minutes in the mechanic shaker and one minute by hand
5. Weigh and record the amount of aggregate left in each sieve

A.2 Specific Gravity of Soil Solids by Water Pycnometer (ASTM D854-02)

1. Measure the mass of a clean dry pycnometer
2. Fill the pycnometer with deaired water above the calibration mark, and level it by removing water with a pipette
3. Record the mass of pycnometer + water
4. Place a mercury thermometer in the pycnometer, and record the temperature of water
5. Calculate the calibrated volume of the pycnometer as follows:

$$V_P = \frac{\left(M_{PW,C} - M_P\right)}{\rho_{W,C}}$$

6. Place approximately 60g of each sample inside an oven at 110 ± 5°C for 24 hours

7. Remove the specimens from the oven, and spoon them into the pycnometer with a funnel
8. Rinse and clean soil particles remaining on the funnel using deionized water
9. Add water to a depth of ? to ½ of the pycnometer main body, and agitate it until slurry is formed
10. Remove entrapped air from the slurry by agitating continuously under vacuum for two hours
11. Fill the pycnometer with deaired water to the calibration mark, and weigh it
12. Place the mercury thermometer in the pycnometer, and record the temperature of the water + soil
13. Calculate the mass of the pycnometer and water at the test temperature as follows:

$$M_{PW,t} = M_P + \left(V_P \cdot \rho_{W,t}\right)$$

14. Calculate the specific gravity of the soil at the test temperature as follows:

$$G_t = \frac{\rho_S}{\rho_{W,t}} = \frac{M_S}{\left[M_{PW,t} - \left(M_{PWS,t} - M_S\right)\right]}$$

15. Calculate the specific gravity of the soil at 20°C as follows:

$$G_{20^\circ C} = KG_t$$

where K is a temperature coefficient provided in Table 2 of ASTM D 854–02

A.3 Maximum Index Density (ASTM D 4253 – 00)

1. Measure the mold dimensions, and compute the average of three measurements of height and diameter to obtain the volume (See Figure A.1)

2. Mix the oven-dry sand to minimize segregation
3. Fill the mold soil using a scoop to about one inch over the mold height
4. Place the surcharge on the soil surface (13.1kPa, 1.9lb/in^2)
5. Secure the mold on the standard vibration table (0.013in, 60Hz), and vibrate it for eight minutes
6. Remove the surcharge and upper part of the mold, and weigh the specimen
7. Calculate the mass of mold + specimen, and determine the mass of the specimen
8. Calculate the minimum void ratio as follows:

$$e_{\min} = \frac{\rho_{W,20^\circ} G_{S,20^\circ}}{\rho_{d\max}} - 1$$

$$\rho_{d\max} = \frac{M_S}{V}$$

$$\rho_{W,20^\circ} = 0.99821\, g/cc$$

A.4 Minimum Index Density (ASTM D 4254 – 00)

1. Mix the oven-dry sample to minimize segregation.
2. Fill the mold with soil using a funnel as closed to the specimen as possible (1/4in) but without direct contact with the poured soils. Move the funnel in a spiral pattern from the perimeter to the center until an elevation just over the mold height is attained.
3. Remove the upper part of the mold, and weigh the specimen carefully
4. Calculate the mass of mold + specimen, and determine the mass of the specimen
5. Calculate the maximum void ratio as follows:

$$e_{\max} = \frac{\rho_{W,20^\circ} G_{S,20^\circ}}{\rho_{d\min}} - 1$$

$$\rho_{d\min} = \frac{M_S}{V}$$

$$\rho_{W,20^\circ} = 0.99821\, g/cc$$

A.5 Particle Shape Identification

1. Take representative particles from each sieve size and place them in separate dark non reflective sample holders
2. Place the sample holders under the Leica MZ6 stereomicroscope
3. Take a digital image by the microscope camera
4. Identify 30 representative particles from a specimen and number on the images
5. Compare each numbered particle with the chart (Krumbein and Sloss 1963; See Figure A.2), and record the sphericity and roundness of the best fitting particle
6. Define the corresponding sphericity and roundness of the specimen as the average of the 30 individual measurements summary of the procedure appears in Figure A.3

Reference: Krumbein, W. C., and Sloss, L. L. (1963). *Stratigraphy and Sedimentation*, W. H. Freeman and Company, San Francisco

A.6 Angle of Repose

1. Pour sands through a funnel into a transparent plaxi glass rectangular container (See Figure A.4a)

2. Fill roughly one third of the container's height with sand, and remove the funnel, and tilt the container until its axis is nearly horizontal
3. Bring the container back to vertical very gently
4. Set a digital camera at the side of the container, and align it to capture a side view of the pile
5. Import the picture into AutoCAD as a raster image
6. Draw lines along the material's slope (see Figure A.4b)
7. Record the angle between the fitted lines

A.7 Flow Test of Hydraulic Cement Mortar (ASTM C 1437-01)

1. Fill the flow mold on the middle of the table with mortar to mid height (See Figure A.5a)
2. Tamp the mortar 20 times (enough pressure to ensure uniform fill)
3. Fill to full height
4. Tamp the mortar 20 times
5. Scrap away mortar above the mold (See Figure A.5b)
6. Remove the mold and drop the table 25 times in 15 sec
7. Measure the distance from the edge of the table to the mortar along the 4 lines subscribed in the table.

$$F = \frac{D - D_0}{D_0} \times 100[\%]$$

where F is the flow, D is the horizontal spread of mortar pile at 25 drops, and D_0 is the initial diameter of mortar pile.

A.8 P-Wave Velocity Measurement

1. Set up the Rapid system, filter, source generator and computer
2. Access computer program RS Scope and retrieve the mortar setup
3. Coat the transducers with silicone
4. Set the cube between the transducers in a face perpendicular to the tamping direction (See Figure A.6a)
5. Use the computer program RS Scope to acquire the signal (See Figure A.6b)

A.9 Unconfined Compressive Strength Test (ASTM C 109)

1. Pour water in the Mixing Bowl
2. Slowly add cement while mix during 30 seconds
3. Add sand over 30 seconds while mixing (slow rate)
4. Mix for 30 seconds more
5. Scrap the side whit the metal spatula 15 seconds
6. Cover the bowl and allow mortar to be set for 75 seconds
7. Continue mixing for 60 seconds
8. Fill three cubical molds to a half with mortar
9. Tamp each mold 32 times in four rounds as described in Figure A.7, complete one cube before passing to the next
10. Fill the molds to full height
11. Tamp again each mold 32 times

12. Scrap excess mortar and place the molds in an airtight container

13. Detach the specimen from the mold after seven days ± three hours

14. Clean the surfaces of the specimen to make a good contact with the testing machine

15. Apply load at a rate of 2000 lb/min to failure (See Figure A.8)

16. Record its peak strength (See Figure A.9)

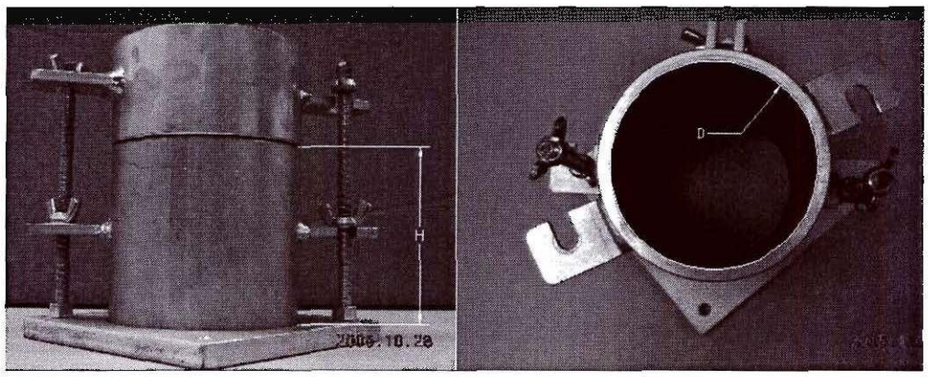

Figure A.1 Mold dimensions (D=100.6mm, H=81.9mm)

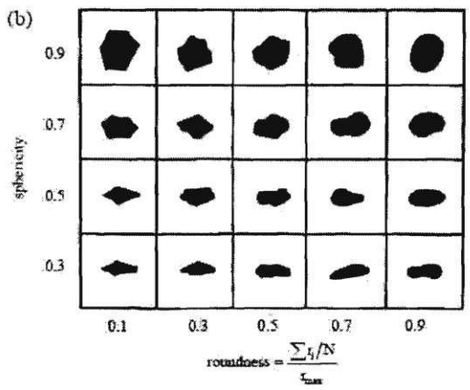

Figure A.2 Particle shape determination and sphericity (Krumbein and Sloss 1963)

Particle ID	Sphericity	Roundness
1	0.7	0.3
2	0.5	0.1
3	0.3	0.7
4	0.3	0.5
5	0.5	0.5
6	0.7	0.3
...	...	...
25	0.5	0.3
26	0.5	0.3
27	0.7	0.3
28	0.3	0.5
29	0.7	0.5
30	0.7	0.3
Average	**0.64**	**0.35**

Subangular

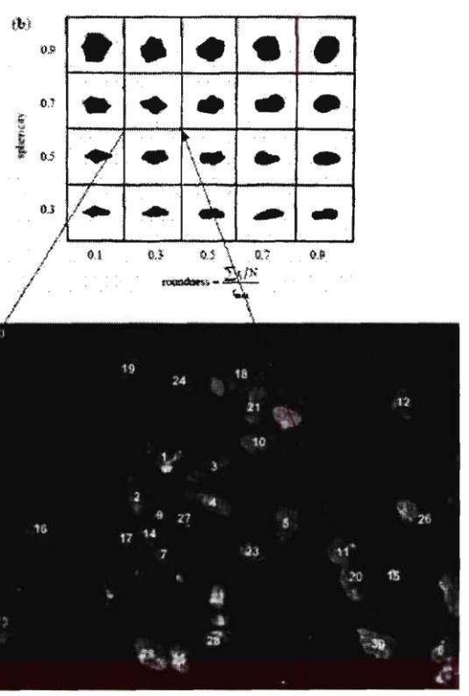

Figure A.3 Procedures to determine particle roughness and sphericity

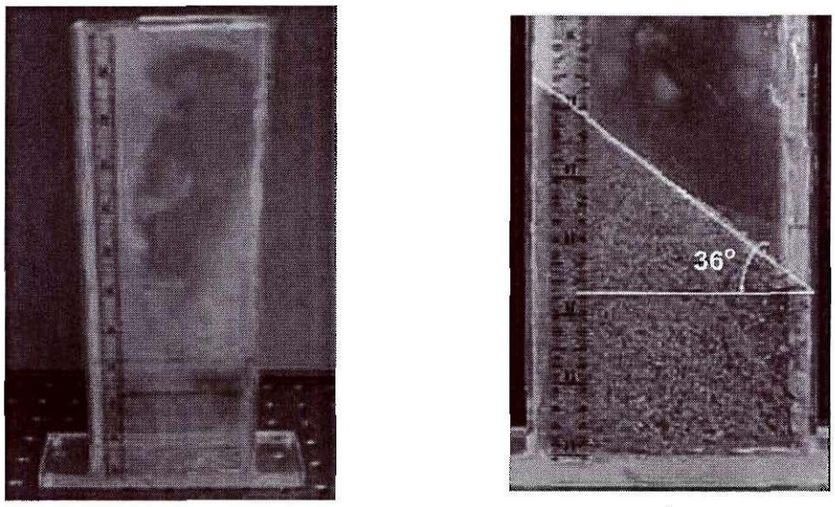

(a) (b)

Figure A.4 Angle of repose measurement with AutoCAD: (a) rectangular plaxi glass container, (b) GDOT standard sand

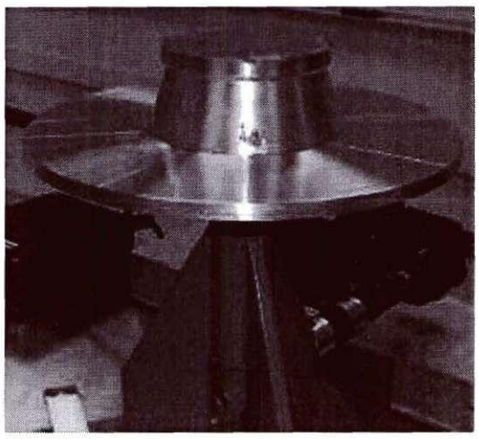

(a)

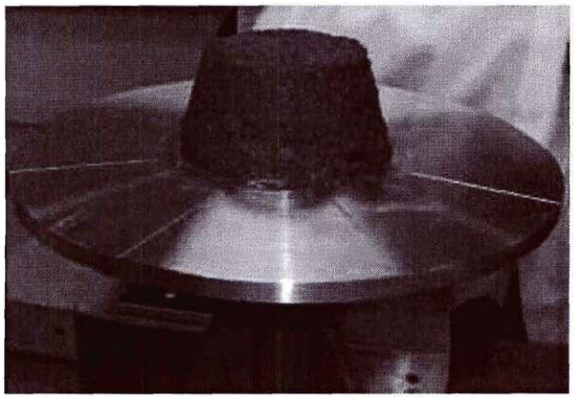

(b)

Figure A.5 Flow test: (a) Preparation of mortar with mold, (b) shape of mortar after removing the mold

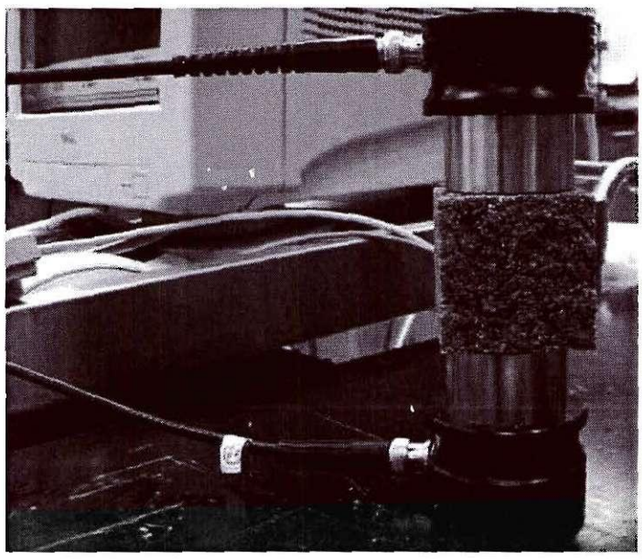

(a)

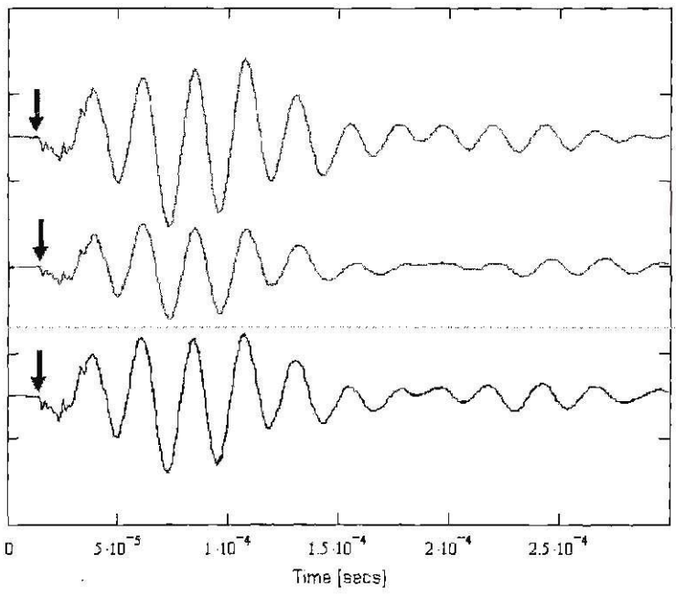

(b)

Figure A.6 P-wave velocity measurement: (a) Experimental setup, (b) examples of P-wave signals: GDOT standard sand mix (W/C=0.46, FA/C=2.0)

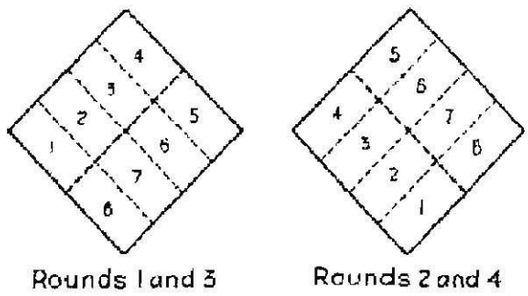

Figure A.7 Tamping pattern for cubic hydraulic mortar specimen (ASTM C 109)

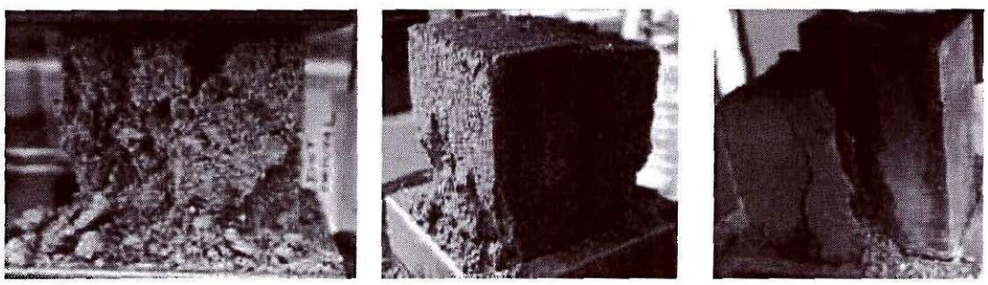

Figure A.8 Examples of broken specimens after unconfined compressive testing

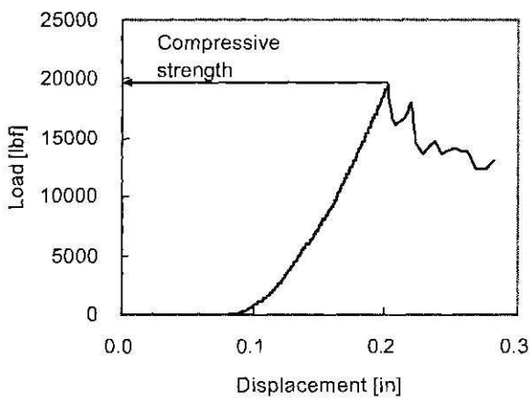

Figure A.9 Load-displacement curve of unconfined compressive test
(Crushed granite sand type I batch #7 Cube#1)

Appendix B. Natural Moisture Content, Strength and Flow

Moisture absorbed inside fine aggregates is difficult to be avoided in the nature. The Georgia DOT standard sand in this study has about 4.5% of water content. The effects of such initial moisture on the compressive strength and flow are investigated. Table B.1 summarizes the blending ratios. A reduced amount of water is mixed in naturally moist sand mortar to maintain the same total water content with the oven-dried sand mortar.

B.1 Compressive Strength

As evidenced by the data in Table B.2 and Figure B.1, there are no significant differences in compressive strength due to initial moisture content of fine aggregates. Curing process provides enough time for cement hydration reactions to take place over the entire specimen; any differences would be more relevant to short term phenomena.

B.2 Flow

The naturally moist sand mortar shows higher flow than the oven-dried sand mortar when the volume factor $V_P/V_{VFA} \leq 1.0$. Absorbed water surrounding moist sands separates fine aggregates and cement paste in the moist sand mortar (See Figure B.2 and Table B.3). The absorbed water effect becomes negligible when enough paste is mixed, so no clear differences are observed in the flows of mortar with high ratio of V_P to V_{VFA}.

Table B.1 Corrected batch proportions considering natural moist in sands (w=4.53%)

Batch #	W/C	FA/C	Water [g]	Cement [g]	Aggregate [g]
2	0.46	2.00	251.05	687.50	1440.20
3	0.50	2.00	278.55	687.50	1440.20
4	0.54	2.00	306.05	687.50	1440.20
7	0.50	2.75	184.80	500.00	1440.20
8	0.54	2.75	204.80	500.00	1440.20
12	0.54	3.25	163.26	423.08	1440.20

Table B.2 Compressive strength (average of 3 test cubes each) with the corresponding volume factors

Batch	Strength (psi)		V_{Paste}/V_{VFA}
	Naturally moist	Oven-dried	
2	5503	5501	1.30
3	5489	5531	1.37
4	4588	4334	1.43
7	5020	4990	0.99
8	4123	4258	1.04
12	3512	1916	0.88

Table B.3 Flow (average of 3 test cubes each) with the corresponding volume factors

Batch	Flow (%)		V_{Paste}/V_{VFA}
	Naturally moist	Oven-dried	
2	108	103	1.30
3	120	115	1.37
4	135	126	1.43
7	71	52	0.99
8	105	82	1.04
12	77	31	0.88

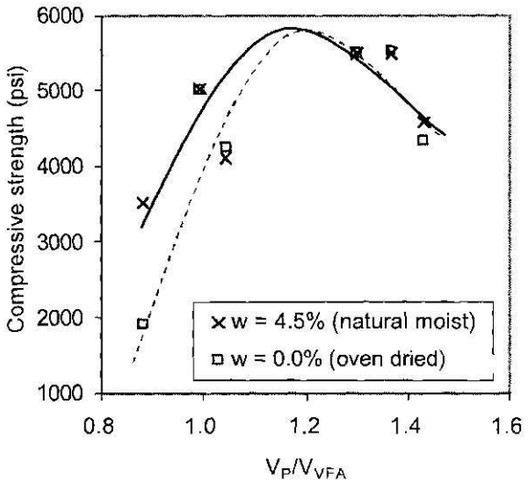

Figure B.1 Compressive strength vs. the volume factor V_P/V_{VFA} ratio
(Naturally moist sand mortar and oven-dried sand mortar)

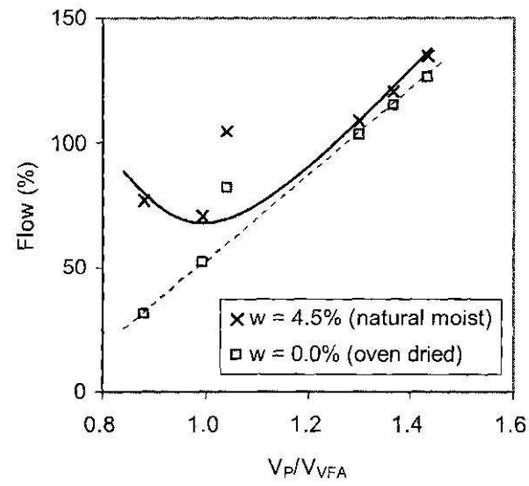

Figure B.2 Flow vs. the volume factor V_P/V_{VFA} ratio
(Naturally moist sand mortar and oven-dried sand mortar)

Appendix C. Mixing Methods, Strength and Flow

Mechanical mixing can apply more energy in mixing and crushing cement clumps with water and fine aggregates than hand mixing. Thus, the mortar mixed with blending machine can have higher workability and strength. Yet, such a theory can be applied only when the mortar is "wet" because the mortar in "dry" side shows lower strength and higher flow when lower paste in mortar. Comparative tests are conducted for the crushed granite sand type I mortar and results are summarized in Figure C.1 and C.2.

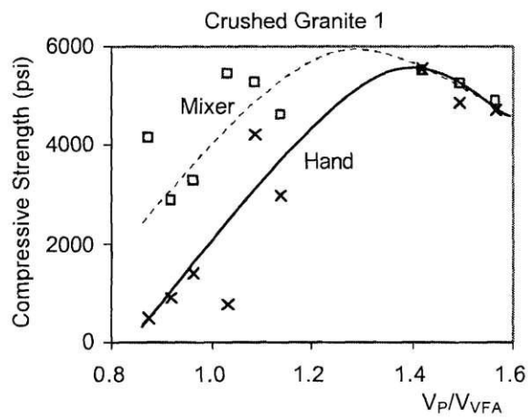

Figure C.1 Compressive strength vs. volume factor V_P/V_{VFA} (Comparison between hand mixed and machine mixed batches made of crushed granite sand type I)

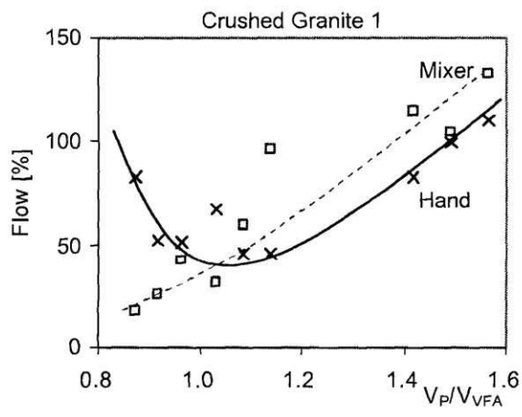

Figure C.2 Flow vs. volume factor V_P/V_{VFA} (Comparison between hand mixed and machine mixed batches made of crushed granite sand type I)